Quantum phases driven by strong correlations

Silke Paschen[1,2] ✉ *and Qimiao Si*[2] ✉

Abstract | It has long been thought that strongly correlated systems are adiabatically connected to their non-interacting counterpart. Recent developments have highlighted the fallacy of this traditional notion in a variety of settings. In this Review, we use a class of strongly correlated electron systems to illustrate the type of quantum phases and fluctuations that are created by strong correlations. Examples include quantum critical states that violate the Fermi liquid paradigm, unconventional superconductivity that goes beyond the Bardeen–Cooper–Schrieffer framework, and topological semimetals induced by the Kondo interaction. We assess the prospects for designing other exotic phases of matter by using alternative degrees of freedom or alternative interactions, and discuss the potential of these correlated states for quantum technology.

In simple metals such as copper and aluminium, mobile electrons experience mutual Coulomb interactions that are small compared with their kinetic energy. It is then adequate to perturbatively treat the effect of the interactions starting from textbook one-electron theories. When, by contrast, the Coulomb interaction reaches the same order as the kinetic energy or becomes even larger, the systems are strongly correlated. They represent a challenge to simple theories, given that non-perturbative effects of the interactions may become essential. Yet such strongly correlated quantum materials provide an exciting ground that is rich with new physics and abundant in opportunities for discoveries. A particularly promising setting for emergent phenomena appears near continuous zero-temperature phase transitions. They generate quantum critical fluctuations which, in turn, may produce exotic excitations and new quantum phases. Indeed, strongly correlated electron systems have been providing a rich setting for conceptual and theoretical advances. Examples include highly entangled phases of matter[21] and quantum critical points (QCPs) that go beyond the Landau framework[22–24].

This Review is motivated by a number of developments in the field of strongly correlated electron systems that have created excitement in the community and may also stimulate progress in adjacent fields. One of the key open problems is the understanding of high-temperature superconductivity. Much effort, both experimental and theoretical, has been devoted to uncovering what kind of quantum critical fluctuations, if any, drive the Cooper pairing. The observation of a change in the carrier density at the pseudogap critical point in a cuprate superconductor near optimal doping[1] suggests a compelling link to the selective 4*f* Mott transition in heavy fermion compounds across Kondo-destruction QCPs[2–7], which may also feature a dome of high-temperature superconductivity[8]. A quantum critical charge delocalization transition thus appears as a promising candidate. Similar phenomena are observed in an organic superconductor[9] and, possibly, in twisted bilayer graphene[10], further underpinning the need for a unified understanding.

In quantum materials, strong correlations often manifest via their spin degree of freedom. However, there is increasing recognition of the importance of other building blocks to the low-energy physics. A case in point is the role played by orbitals. Being well established in transition metal oxides[11], orbitals are frequently entwined with other degrees of freedom and may thus reveal their character only in low-energy excitations. Examples are the iron-based superconductors[12], the hidden order phase in URu_2Si_2 (REF.[13]) or the sequential localization in an SU(4)-type heavy fermion system[14]. Finally, there is a surge of work on the interplay of strong correlations and topology. There has been particular focus so far on quantum spin liquids, topological insulators and semimetals in transition metal compounds[15–17], Weyl–Kondo semimetals in heavy fermion systems[18,19], and renormalized Dirac fermions in twisted bilayer graphene[10]. It is expected that in the strong correlation regime, a wealth of entirely new phases — not adiabatically connected to those known in non-interacting systems — will be discovered, and push the frontiers of science much like the discovery of the fractional quantum Hall effect[20] did in two-dimensional (2D) insulators.

In FIG. 1 we introduce different materials classes hosting strongly correlated electrons. Prominent representatives are the cuprate high-T_c superconductors[25], ruthenates and other transition metal oxides[11], heavy fermion systems[26], iron-based superconductors[12], organics[9]

[1]*Institute of Solid State Physics, Vienna University of Technology, Vienna, Austria.*

[2]*Department of Physics and Astronomy, Rice Center for Quantum Materials, Rice University, Houston, TX, USA.*

✉*e-mail: paschen@ifp.tuwien.ac.at; qmsi@rice.edu*

https://doi.org/10.1038/s42254-020-00262-6

Key points

- Quantum criticality accumulates entropy, turns quantum matter soft, and makes it prone to the development of exotic excitations and new emergent phases.
- Strongly correlated electron systems can exhibit quantum critical points with fluctuations beyond those of the vanishing Landau order parameter, as exemplified by electronic localization–delocalization transitions associated with Kondo-destruction quantum criticality.
- Quantum phases are enriched by the interplay between strong correlations, geometrical frustration, entwined degrees of freedom and hybrid interactions.
- Strong correlations interplay with spin–orbit coupling and space-group symmetry to drive topological states of matter, as exemplified by Weyl–Kondo semimetals.
- In quantum materials, we let nature work for us and reveal new physics that we might never have imagined. This leads to models and concepts that could then be studied in artificial settings such as ultracold atomic and photonic systems, and models for gravity.

and low-dimensional materials[10]. The relevant electron orbitals in these systems are typically the *d* or *f* orbitals, which, unlike the *s* or *p* orbitals, keep some degree of localization in the solid and thus lead to enhanced Coulomb interaction and reduced bandwidths. In addition, at appropriate filling, they give rise to localized moments. In this Review, we begin by describing how these features lead to the low-energy degrees of freedom which — together with the conduction electrons, phonons and other excitations present also in weakly correlated cases — are the building blocks of correlated matter. The mutual interactions between them, together with the symmetry defined by the hosting crystal structure, result in an overwhelming richness in physical properties. A key goal of the quantum materials community is to trace these properties back to the various magnetic, superconducting, and topological phases (for representative phase diagrams, see Supplementary Fig. 1), and transitions between them, to ultimately allow the creation of functionality via materials design. A viable approach towards this goal is to apply non-thermal control parameters such as pressure or magnetic field to a given material to tune it across its various phases, and to follow the evolution of its properties. We will show that the extreme 'softness' (responsiveness) of heavy fermion compounds to external parameters makes them particularly suitable for such studies. We then discuss the quantum phases and fluctuations that have been discovered by such tuning investigations on heavy fermion systems where the Kondo coupling and the Ruderman–Kittel–Kasuya–Yosida (RKKY) interaction are competing. In the following section, we describe new horizons in the field, addressing the potential of alternative tuning parameters, additional degrees of freedom and interactions beyond the canonical spin–conduction electron form, and the role of topology. The implications of the insight gained from studying heavy fermion systems on other classes of correlated materials and, more generally, correlated states of matter, are then discussed. We close with an outlook and some open questions.

Building blocks of correlated matter

In strongly correlated electron systems, the 'onsite' Coulomb repulsion between electrons associated with the same lattice site is comparable to or larger than the width of the underlying non-interacting energy band. Thus, such atomic-level electron–electron interactions cannot be taken as a mere perturbation. Instead, they are more appropriately treated at the zeroth order, and a set of atomic levels ensues. These atomic levels are energetically so far apart that only the lowest energy levels can directly influence the thermodynamic or (energy/time-resolved) dynamical properties at low energies. The quantum numbers of these low-lying atomic levels, together with those of delocalized excitations such as itinerant electrons or acoustic phonons, specify the fundamental degrees of freedom — the building blocks — of the correlated system (FIG. 1).

A familiar example is the Mott insulator in 3*d* transition metal systems. In the simplest case, where only one 3*d* orbital is important for any given lattice site, there is on average one electron per orbital (half-filled case), and the onsite Coulomb repulsion U is larger than the bare (underlying, non-interacting) electron bandwidth. The lowest-energy atomic level, a doublet with the degeneracy given by the spin degree of freedom, is then occupied by a single electron; this corresponds to a localized quantum spin $S = 1/2$. Accessing the high-energy atomic levels amounts to creating or removing an electron from the singly occupied doublet. Because this costs an energy of the order of $U/2$, these are high-energy electronic excitations (responsible for the Hubbard bands) and do not directly contribute to the low-energy properties. They do, however, mediate superexchange interactions between the localized moments.

Another example arises in the 4*f*-electron-based heavy fermion systems. The strong onsite Coulomb repulsion of the 4*f* electrons, in combination with the large spin–orbit coupling and crystal electric field effects, frequently leads to a Kramers doublet as the lowest-lying atomic level, again giving rise to localized moments of effective spin $S = 1/2$. These moments interact with a separate band of *spd* electrons, in the form of an antiferromagnetic Kondo interaction, and with each other through an RKKY spin-exchange interaction that is mediated by the spin polarization of the conduction electrons[27].

The presence of these well-defined building blocks and their interactions has several implications. The Kondo and RKKY energy scales are small — orders of magnitude smaller than the bare conduction electron bandwidth (see Supplementary Box 1). Such energy scales can be substantially modified by laboratory-scale pressures or magnetic fields, for example, making heavy fermion systems highly tunable and, in turn, a prototype model setting for studying quantum criticality. In addition, the clear understanding of the building blocks aids sharp theoretical analyses. Thus, we use heavy fermion systems as a prototype setting for our discussion of tuning and quantum criticality.

Tuning heavy fermion systems

There are many correlated materials to be explored. This is due to the large number of *d* and *f* elements in the periodic table which are (at least in bulk materials) generally constituents of correlated materials, and the numerous crystal structures of binary, ternary, quaternary and so

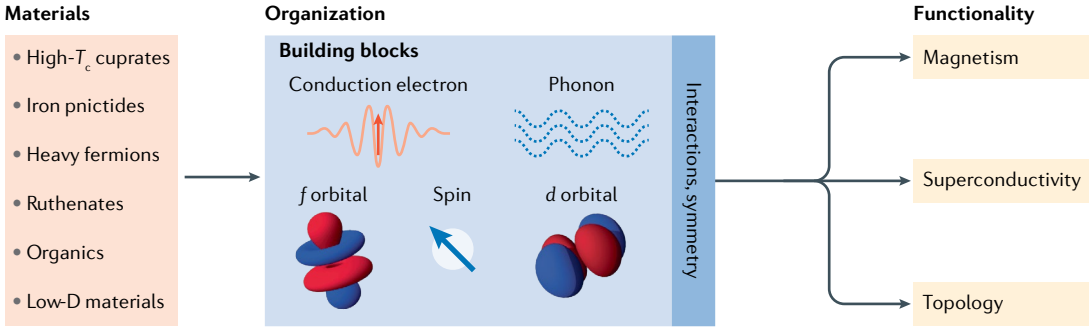

Fig. 1 | **Functionality of strongly correlated materials.** Selected classes of strongly correlated materials, and how interactions between their low-energy degrees of freedom ('building blocks') and symmetry may lead to different functionalities. Examples of the rich resulting phase diagrams for several of these materials classes are shown in Supplementary Fig. 1.

on compounds that may combine these elements with each other and with *s* and *p* elements. Indeed, it is important to sample this huge phase space of correlated materials at vastly different positions, to discover overarching principles and test for their universality. However, an alternative strategy to this 'zoology approach' is a 'tuning approach'. It is to (quasi-)continuously monitor the evolution of a given system's properties along a specific path in the phase space. Such tuning studies have proven to be instrumental in advancing the field (FIG. 2).

One goal of tuning studies is to establish the different phases or ground states that a given material system can adopt. A few examples of phase diagrams, displaying the phase transition temperatures of the system as function of a non-thermal tuning or control parameter, are shown in Supplementary Fig. 1. These phase diagrams provide guidance to the understanding of the respective material and allow one to relate the observed physical properties to the different phases, or even to certain parts of a given phase (such as the centre or border of a phase). Typical tuning parameters are chemical substitutions within a family of isostructural compounds, doping as a special case thereof, or the application of external parameters such as pressure or magnetic field. Depending on the materials class, modest or very large variations of these parameters may be needed to appreciably change the properties of the system.

A materials class that is particularly responsive to such stimuli is heavy fermion compounds. This is attributed to the presence of (at least) the aforementioned two competing energy scales, the Kondo and the RKKY interaction[27]. As already considered in the simplified case of a 1D Kondo lattice, tipping the balance between the two scales is expected to tune the system from an antiferromagnetic to a paramagnetic state[28]. Indeed, numerous studies on heavy fermion metals have identified such transitions[29–34].

Vital for establishing trends, and thus for laying the ground for a universal understanding of the observed properties, was the identification of a few simple, experimentally well defined and meaningful characteristics of the studied materials. Since the 1970s (REF.[35]), it has been known that many heavy fermion metals show Fermi liquid properties at low temperatures. The quantities most commonly measured in these materials are the electrical resistivity (ρ), magnetic susceptibility (χ) and specific heat (c). The Fermi liquid forms[27] of these are $\rho = \rho_0 + AT^2$, $\chi = \chi_0$ and $c = \gamma T$, where ρ_0 is the residual resistivity, A the prefactor of the temperature (T)-dependent contribution, χ_0 the residual magnetic susceptibility due to conduction electrons (Pauli susceptibility) and γ the Sommerfeld coefficient. The correlation strength, quantified by the renormalized effective mass m^* of the charge carriers, enters in all three expressions, to first approximation as $A \sim (m^*)^2$, $\chi_0 \sim m^*$ and $\gamma \sim m^*$. As such, the experimental determination of A, χ_0 and γ allows heavy fermion metals to be categorized according to their degree of correlation. Assembling data of numerous heavy fermion metals in plots of γ versus χ_0 and A versus γ confirmed the theoretically expected universal Sommerfeld–Wilson ratio and the Kadowaki–Woods ratio[36]. This can be seen neatly if corrections due to different ground-state degeneracies[37] and effects of dimensionality, electron density and anisotropy[38] are taken into account (FIG. 2a).

Further insight was gained with the discovery that A, χ_0 and γ of even a single given material can be widely varied by the application of external tuning parameters. As illustrated with two examples in FIG. 2b,c, in addition to ranges where the effective mass is continuously (adiabatically) varied as a function of the magnetic field, there are neuralgic points where the effective mass appears to diverge. Clearly, at such points, something extraordinary must be going on, and this is now known to be the presence of a QCP[33]. Quantum critical fluctuations emerging from a QCP lead to temperature dependencies distinct from Fermi liquid behaviour, as discussed in the following section.

Quantum phases and fluctuations

A QCP appears as the ground state of a quantum many-body system smoothly transforms from one state to another (FIG. 3). Typical of the systems we consider in this article is a gradual suppression of an electronic ordered phase (FIG. 3a). Entropy accumulates near a QCP, as can be seen from hyperscaling. The free energy density, with the dimension of energy/volume, is expected to have a singular component of the form $k_B T/\xi^d$ multiplied by a universal scaling function of $|p - p_c|/\xi^{-1/\nu}$. Here ξ is the correlation length, d the spatial dimension, ν the

Sommerfeld–Wilson ratio
The ratio of the (Pauli paramagnetic, temperature-independent) magnetic susceptibility to the linear-in-temperature specific heat (Sommerfeld) coefficient γ.

Kadowaki–Woods ratio
The ratio of the quadratic-in-temperature electrical resistivity coefficient, A, to the square of the linear-in-temperature specific heat (Sommerfeld) coefficient γ.

correlation length exponent and, for concreteness, we consider the tuning parameter δ to be linearly coupled to pressure p. It follows from this scaling form that the Grüneisen ratio as a function of p is maximized near p_c (REF.[39]) and so is the entropy S (more precisely, the ratio S/T) for a sufficient low T (FIG. 3b)[40].

The enhanced entropy makes the electron system particularly soft (more responsive), which promotes the

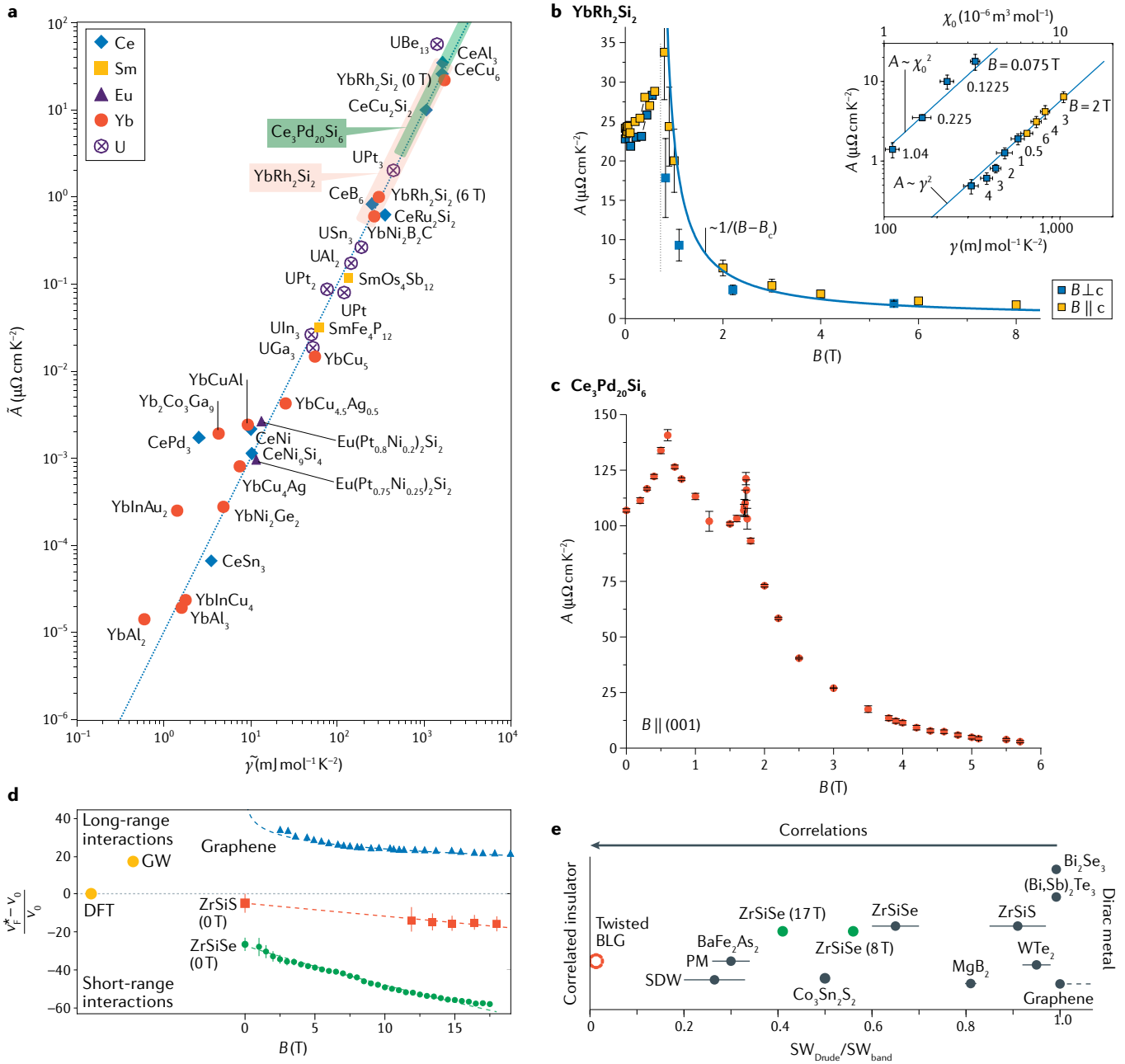

Fig. 2 | **Tuning correlation strength. a** | Generalized Kadowaki–Woods plot, including ranges of A coefficient reached in experiments on the heavy fermion compounds $YbRh_2Si_2$ from panel **b** and $Ce_3Pd_{20}Si_6$ from panel **c** in shaded areas. Data points and shadings refer to experimental values for $\tilde{A} = A/[N(N-1)/2]$ and $\tilde{\gamma} = \gamma/[N(N-1)/2]$, where N is the degeneracy of the involved local moment state. **b** | The A coefficient of the low-temperature electrical resistivity of $YbRh_2Si_2$ as function of applied magnetic field $B = \mu_0 H$. The inset relates the A coefficient to the Sommerfeld coefficient γ and the Pauli susceptibility χ_0, and confirms the validity of the Kadowaki–Woods and Sommerfeld–Wilson ratios. **c** | The A coefficient of the low-temperature electrical resistivity of $Ce_3Pd_{20}Si_6$ versus B, indicating mass enhancements at two distinct fields. The error bars in **b** and **c** represent standard deviations of Fermi liquid fits (see text). **d** | Fermi velocity, v_F^*, renormalization with respect to the non-interacting value, v_0, from density functional theory (DFT) versus magnetic field for the nodal-line semimetal ZrSiSe, the nodal-loop semimetal ZrSiS, and graphene. The Fermi velocity obtained for ZrSiSe in the GW approximation is larger than that calculated within DFT. **e** | Correlation strength in various topological materials as quantified by the reduced Drude spectral weight compared with the DFT value. The symbol for twisted bilayer graphene (BLG) represents a prediction from the observed insulating state. Error bars in **d** and **e** represent absolute minima and maxima. References for all materials in **d** and **e** other than ZrSiSe are given in REF.[134]. Part **a** is adapted with permission from REF.[37]. Part **b** is adapted with permission from REFS[178]. Part **c** is adapted with permission from REF.[14]. Parts **d** and **e** are adapted with permission from REF.[134].

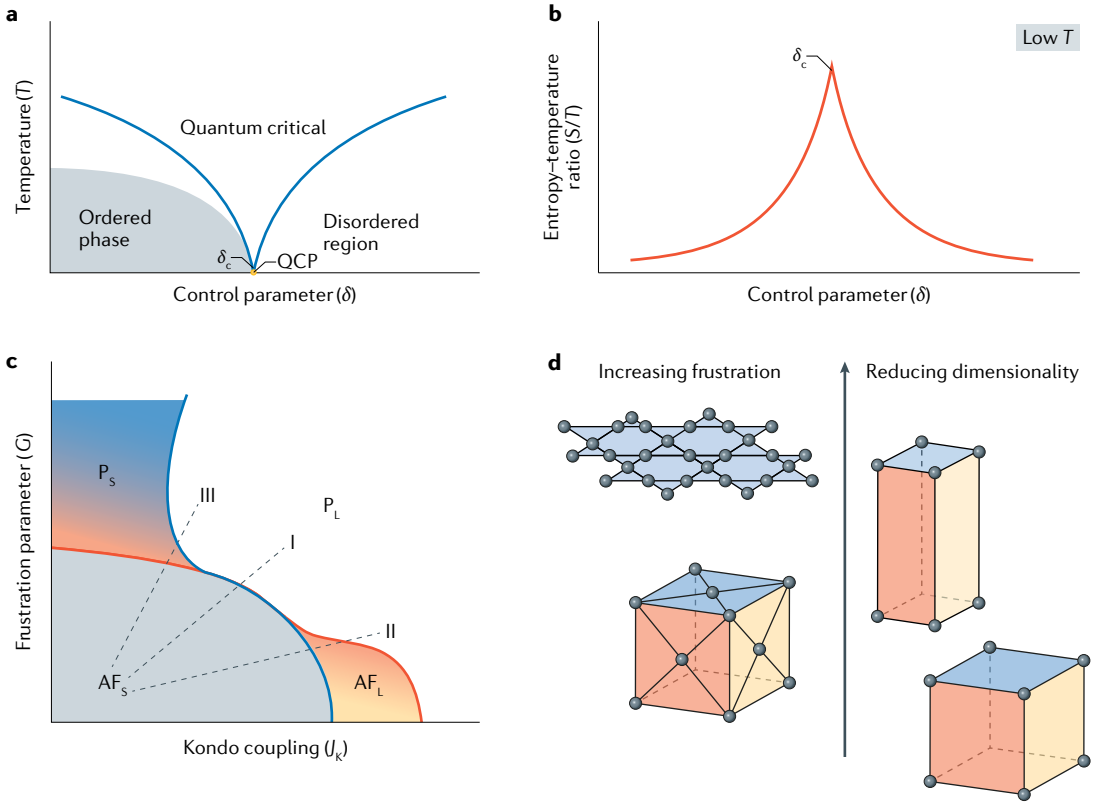

Fig. 3 | **Quantum criticality. a** | Emergence of a quantum critical point (QCP) in the temperature versus tuning parameter (T versus δ) phase diagram. When the Grüneisen ratio is discussed, we consider the case in which δ is linearly coupled to the pressure. The QCP, at zero temperature and $\delta = \delta_c$, represents the point where long-range order is continuously suppressed to zero. **b** | Evolution of the entropy S versus δ, showing that S/T at a low T is peaked near the QCP. **c** | A global phase diagram for heavy fermion metals, where J_K tunes the Kondo coupling and G varies the degree of frustration. P and AF stand for paramagnetic and antiferromagnetic phases, and the subscripts L and S denote the Fermi surface being large and small. **d** | Illustration of variations in the degree of geometrical frustration and in spatial dimensionality. Part **b** is adapted with permission from REF.[40]. Part **c** is adapted with permission from REFS[89,90]. Part **d** is adapted with permission from REF.[6].

nucleation of new excitations and phases. For instance, strongly correlated metals display an unusual temperature dependence of the electrical resistivity at the QCP, reflecting the breakdown of the Landau quasiparticle concept and the ensuing formation of a non-Fermi liquid (strange metal). In addition, unconventional superconductivity often develops near a QCP. As such, quantum criticality can be used as a unifying theme for the description of the often exotic properties across a variety of strongly correlated materials[32,34,41,42].

In practice, quantum criticality often develops in bad metals that are in the vicinity of antiferromagnetic order. A bad metal is specified by its resistivity at room temperature being large, reaching the Mott–Ioffe–Regel limit, which implies the presence of strong electron correlations[43]. Such correlations cause a reduction in the coherent part of the electron spectral weight, as measured by angle resolved photoemission spectroscopy (ARPES)[44] and optical conductivity[45,46]. Because a sufficiently large correlation strength suppresses the coherent electron part, it may lead to an electronic localization–delocalization transition. All these phenomena are exemplified by heavy fermion metals, which are canonical examples of bad metals and in which antiferromagnetic QCPs are especially prevalent[26,29–34]. We thus discuss these systems in what follows.

Quantum criticality. Consider a Kondo lattice (see Supplementary Box 1), comprising a localized moment for each unit cell and a band of conduction electrons (FIG. 4). When the RKKY interaction dominates over the Kondo coupling, the local moments develop static order and form an antiferromagnetic state (FIG. 4d). Deep in this state (far away from the phase boundary), it has been rigorously shown that the Kondo coupling is exactly marginal in the renormalization-group sense[47]. In this case, spin singlets are well established among the local moments, which are detrimental to the development of a Kondo singlet between the local moments and conduction electrons. The Fermi surface is then formed of the conduction electrons only. This is named a small Fermi surface (FIG. 4f).

In the opposite limit, when the Kondo coupling dominates over the RKKY interaction, the local moments form a spin-singlet state with the conduction electrons (FIG. 4e). This is the standard paramagnetic heavy fermion state, characterized by a static Kondo-singlet amplitude. The ensuing Kondo entanglement of the local

Grüneisen ratio
A quantity that is proportional to the ratio of volume thermal expansion to specific heat and diverges at a quantum critical point.

Mott–Ioffe–Regel limit
The condition of maximal scattering in a metal, where the mean free path ℓ becomes comparable to the ratio of 2π to the Fermi wavevector k_F.

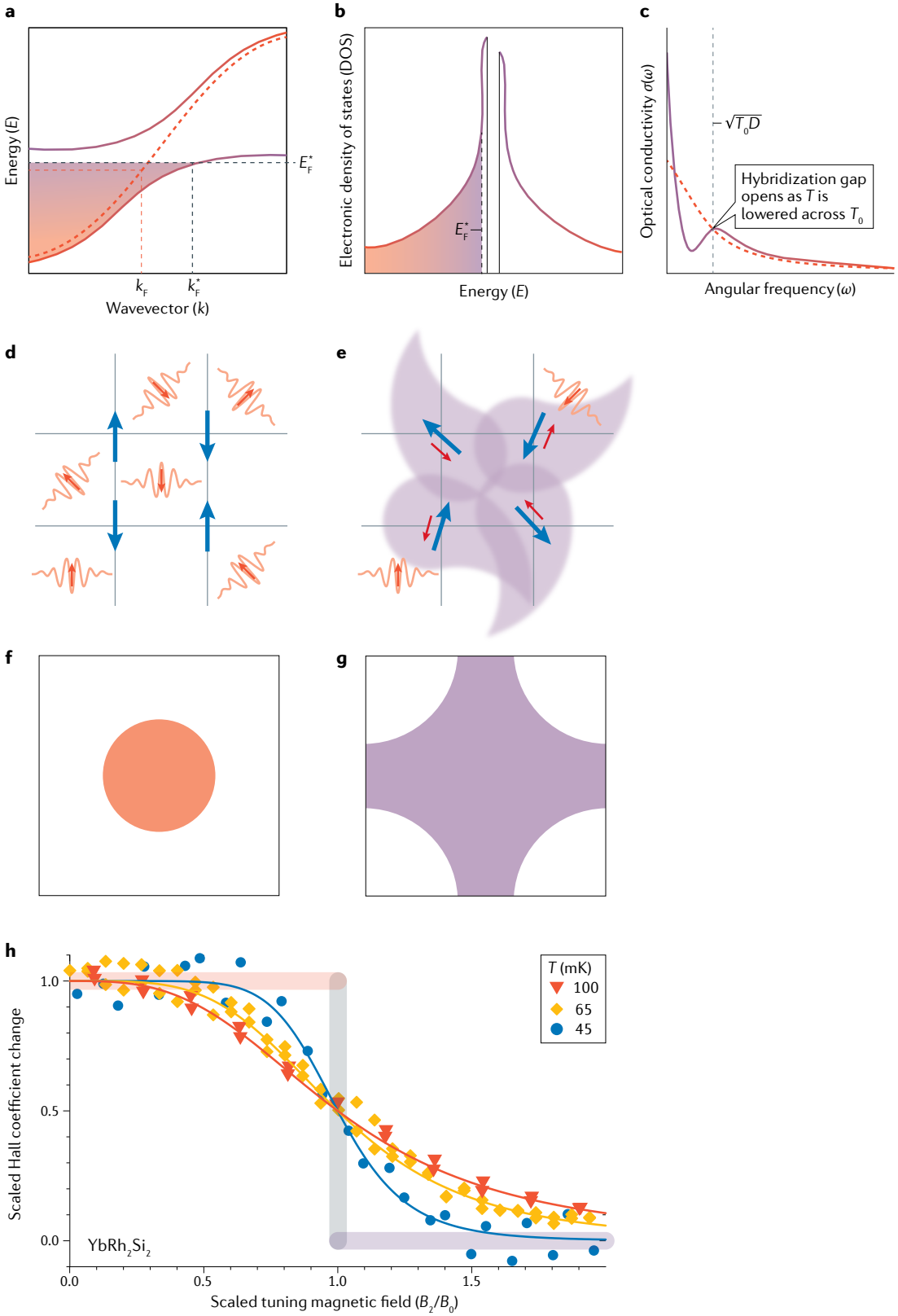

moments with the conduction electrons effectively turns local moments into mobile carriers. A local moment and a conduction electron form a fermionic composite, which corresponds to a delocalized heavy electronic excitation. Its hybridization with the conduction electron band (FIG. 4a–c) produces heavy quasiparticles. Thus, in this limit, the Fermi surface incorporates both the local moments and conduction electrons, and is large (FIG. 4g).

What is remarkable is that the transformation from the small to the large Fermi surface can occur sharply, precisely at a continuous zero-temperature phase transition from an antiferromagnetically ordered to a

◀ Fig. 4 | **Fermi-surface jump at a Kondo-destruction quantum critical point.** **a** | Dispersion of the Kondo screened state in a mean-field description, with hybridized bands resulting from the hybridization between the underlying non-interacting conduction band (red dashed line, with Fermi wavevector k_F) and composite fermions that originate from the local spins (not shown). The increased Fermi wavevector of the hybridized band, k_F^*, reflects the integration of local spins into the Fermi surface (**d**–**h**). **b** | Close-up of the corresponding density of states near the gap. The Fermi energy E_F^* of the hybridized states lies in a region of strongly enhanced density of states. **c** | Signature of the hybridization gap opening due to the Kondo interaction in the optical conductivity σ as function of the angular frequency ω (energy in units of the reduced Planck constant). The development of the hybridization gap as temperature is lowered signifies the initial onset of the Kondo singlet correlations. D is the conduction electron bandwidth. **d** | Kondo lattice model where the Ruderman–Kittel–Kasuya–Yosida (RKKY) interaction dominates over the Kondo coupling. The blue arrows label the local moments, and the red arrows with wavy lines represent conduction electrons. **e** | Kondo lattice model with Kondo screening, where the Kondo coupling dominates. The tadpole-shaped shadings symbolize the heavy quasiparticles. **f** | Small Fermi surface in the RKKY-dominated case shown in **d**. **g** | Large Fermi surface in the Kondo-coupling-dominated case shown in **e**. **h** | Isotherms of the scaled Hall coefficient change as a function of a scaled tuning magnetic field in the heavy fermion compound $YbRh_2Si_2$. The scaled Hall coefficient change is defined as $(R_H - R_H^\infty - mB_2)/(R_H^0 - R_H^\infty)$, where R_H is the linear-response Hall coefficient, R_H^0 and R_H^∞ are the initial and large-field values of a crossover function (red, yellow and blue lines) and mB_2 is a linear background contribution. The scaled tuning magnetic field is the tuning field B_2 normalized by the field B_0 where the crossover occurs. The jump (as seen in the thick lines) represents the limit of extrapolating the data to $T = 0$. Part **c** is adapted with permission from REF.[34]. Part **h** is adapted with permission from REF.[5].

paramagnetic heavy fermion state. In $YbRh_2Si_2$, an antiferromagnet with a low Néel temperature ($T_N = 0.07$ K), application of a small magnetic field weakens the antiferromagnetic order and continuously suppresses it at the critical field B_c (FIG. 2b). Hall effect measurements[3,5] imply a sudden jump in the extrapolated zero-temperature limit, precisely at the QCP (FIG. 4h), consistent with a sudden change from the small to the large Fermi surface. At non-zero temperatures, the Hall results and thermodynamic measurements[48] identify a temperature scale $T^*(B)$ in the temperature–magnetic field phase diagram which, anchored by the Fermi-surface-jumping QCP, characterizes the finite-temperature crossovers. Scanning tunnelling microscopy experiments have provided spectroscopic evidence for the $T^*(B)$ scale[49], where a critical slowing down was evidenced from an analysis of the Kondo resonance linewidth.

Another experimental signature of this effect was revealed by quantum oscillation measurements. $CeRhIn_5$ is an antiferromagnetic metal with a Néel temperature $T_N = 3.8$ K (REF.[50]). Applying pressure weakens the antiferromagnetic order and induces superconductivity[8,51]. In magnetic fields above the superconducting upper critical field H_{c2}, these studies[8,51] reveal an antiferromagnetic QCP near the same pressure p_c where the de Haas–van Alphen (dHvA) frequencies jump and the cyclotron mass diverges[4]. From a comparison with ab initio electronic structure calculations for $LaRhIn_5$ and $CeRhIn_5$ (with the Ce4*f* electrons in the core), it was concluded that the Fermi surface transforms from small at $p < p_c$ to large at $p > p_c$ (REF.[4]).

These striking experimental observations were anticipated by theoretical studies[22–24]. Analysing the Kondo lattice model identified an unusual type of QCP, where a small-to-large Fermi surface jump occurs at the antiferromagnetic–paramagnetic phase boundary[22]. The quantum criticality then captures not only the fluctuations from a suppression of the antiferromagnetic order parameter, but also those associated with a destruction of the static Kondo effect.

Kondo destruction quantum criticality has another salient feature, an ω/T scaling in the spin dynamics (FIG. 5). The collapse of the static Kondo singlet causes the QCP to being described by an interacting fixed point, where the universal physics depends on only k_BT and no other energy scales[22,23]. Calculations on Kondo lattice models based on an extended dynamical mean-field theory have produced such ω/T behaviour in the dynamical spin susceptibility at the Kondo destruction QCP[22,52,53]. This provides the understanding of inelastic neutron scattering experiments on quantum critical $CeCu_{5.9}Au_{0.1}$ (FIG. 5a). Its parent compound $CeCu_6$ is a paramagnetic heavy fermion metal, and a substitution of less than 2% of Cu by Au induces antiferromagnetic order. In $CeCu_{5.9}Au_{0.1}$, the dynamical spin susceptibility displays ω/T (or E/T where $E = \hbar\omega$) scaling with a fractional critical exponent (FIG. 5a), in contrast to what happens in $CeCu_2Si_2$ (FIG. 5b). In β-$YbAlB_4$, B/T scaling has been shown in thermodynamic quantities[54] (FIG. 5c), but dynamical scaling could not yet be tested.

An exciting recent development came from terahertz spectroscopy measurements of the optical conductivity of $YbRh_2Si_2$, which demonstrate ω/T scaling in the charge channel (FIG. 5d)[7]. This was ascribed to the Kondo destruction nature of the QCP. As the Kondo effect also involves the charge degree of freedom, its destruction should also lead to ω/T scaling in the charge sector.

The above features are to be contrasted with expectations for quantum criticality within the Landau framework, which is of spin-density-wave (SDW) type[55–57]. Going across an SDW QCP from the paramagnetic side, the Fermi surface evolves smoothly: it folds by the continuously emerging SDW order parameter. As a result, across this QCP, both the Hall coefficient and the quantum oscillation frequencies vary smoothly. Moreover, the SDW QCP is described by a Gaussian fixed point that is accompanied by a dangerously irrelevant variable. As a result, an effective energy scale other than k_BT is generated and ω/T scaling is violated.

Following the traditional description of the nearly ferromagnetic quantum fluctuations in liquid ^{3}He (REF.[58]), the SDW-type QCP is discussed for purely itinerant electron systems. In heavy fermion compounds, local moments are part of the building blocks for the low-energy physics. It has been stressed that to describe the Kondo destruction QCP it is essential to treat the dynamical competition between the RKKY and Kondo interactions. For instance, while the static Kondo singlet amplitude vanishes as the Kondo destruction QCP is approached from the paramagnetic side, the Kondo correlations at non-zero frequencies smoothly evolve across the QCP[53,59]. This effect is essential for the stability of the Kondo-destroyed phase and also provides the understanding of a mass enhancement in that phase.

In view of this dynamical competition between the RKKY and Kondo interactions, it follows that even in heavy fermion metals described by an SDW QCP at the lowest energies, the Kondo destruction crossover scale T^*, although non-zero, can still be considerably smaller

de Haas–van Alphen (dHvA) frequencies
Characteristic frequencies in quantum oscillation measurements of the magnetic susceptibility that characterize information about the material's Fermi surface.

ω/T scaling
The collapsing of the dependence on the energy ω (in units of the reduced Planck constant) and temperature T in terms of their ratio ω/T.

dangerously irrelevant variable
A term in the renormalization-group (RG) treatment of a many-body system, denoting a variable that is irrelevant in the RG sense but provides leading contributions to certain physical quantities of the system.

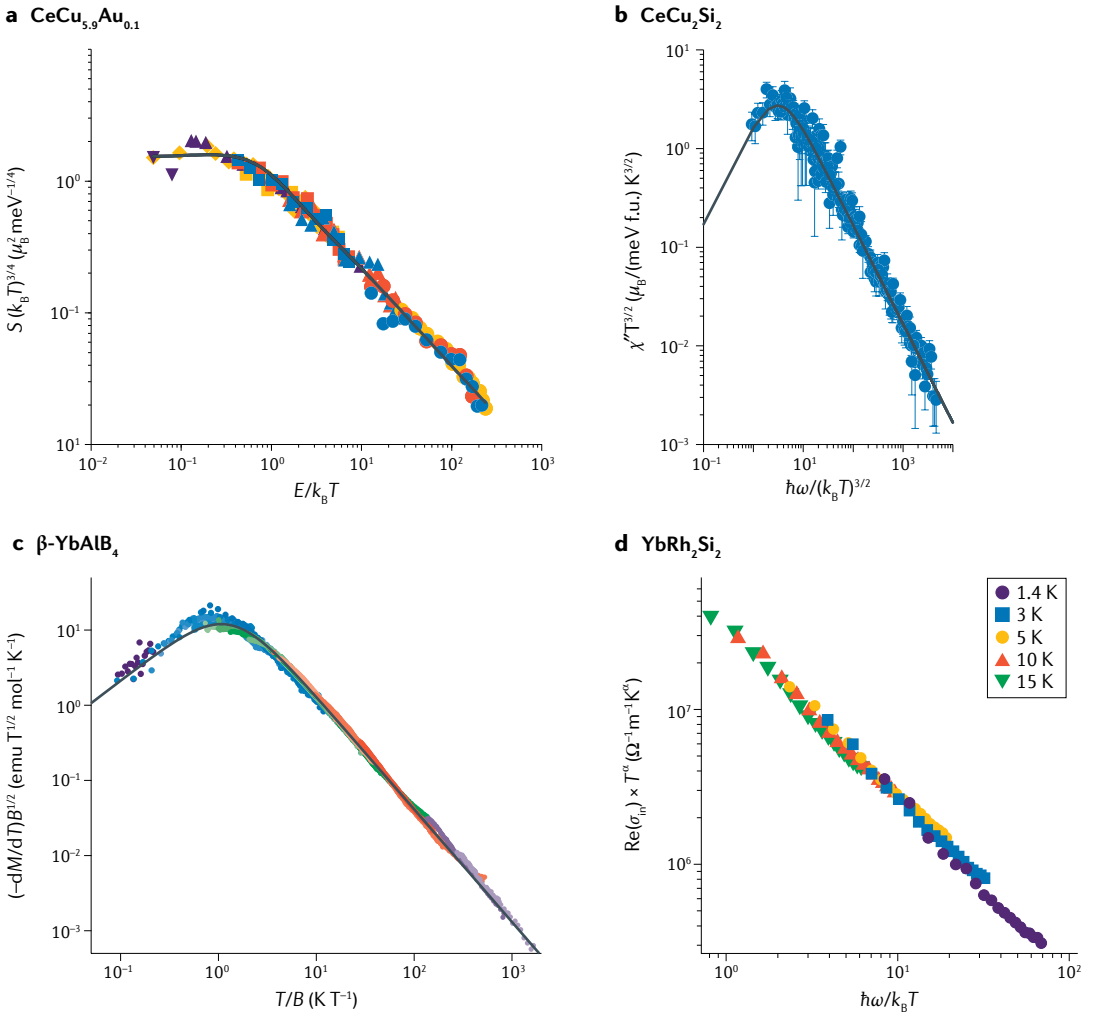

Fig. 5 | **Quantum critical scaling. a** | Dynamical scaling in the spin dynamics of $CeCu_{5.9}Au_{0.1}$. *S* is the intensity of the scattered neutons. The different symbols represent data taken at different critical wavevectors, with temperatures ranging between 80 mK and 8 K and energy transfers between 15 μeV and 2 meV. **b** | Dynamical scaling of the spin dynamics of $CeCu_2Si_2$ described by a spin-density wave model. f.u. stands for formula unit. **c** | *T*/*B* scaling of d*M*/d*T* in β-$YbAlB_4$. The colours of the data points refer to magnetic fields varying between 0.3 mT and 6 T and temperature ranging from 25 mK to 4 K. **d** | *ω*/*T* scaling in the optical conductivity of $YbRh_2Si_2$. *S* is the neutron scattering intensity, χ'' the imaginary part of the dynamical susceptibility, *M* the static magnetization, $\mathrm{Re}(\sigma_{in})$ the real part of the intrinsic optical conductivity, *E* and $\hbar\omega$ the energy transfer (the latter in units of the reduced Planck constant), *T* the absolute temperature, k_B the Boltzmann constant and $B = \mu_0 H$ the applied magnetic field. Part **a** is adapted with permission from REF.[2]. Part **b** is adapted with permission from REF.[61]. Part **c** is adapted with permission from REF.[54]. Part **d** is adapted with permission from REF.[7].

than the bare Kondo temperature scale T_K^0 (the putative Kondo temperature scale in the absence of the competition from the RKKY interaction)[60]. In this case, there is an extended temperature range ($T^* < T < T_K^0$) over which Kondo destruction quantum criticality should dominate the singular physics. For instance, in $CeCu_2Si_2$, the dynamical spin susceptibility follows the $\omega/T^{3/2}$ scaling form predicted for a 3D SDW QCP (FIG. 5b)[61], corresponding to a $T^{3/2}$ relaxation rate. However, this rate becomes linear in *T* already at 1 K and above, pointing to $T^* \sim 1$ K and a sizable temperature range, $T^* < T < T_K^0 \sim 20$ K where the dynamics may be described by Kondo destruction physics; additional ways to ascertain this possibility are needed.

These developments establish antiferromagnetic heavy fermion metals to be a prototype setting for quantum criticality beyond the Landau framework. The fact that such a form of unconventional quantum criticality takes place at a transition between two conventional phases has motivated studies of beyond-Landau QCPs in the context of quantum magnets[62]. From the correlated electron perspective, Kondo destruction signifies an electronic localization–delocalization transition. Indeed, it has been shown that the Kondo destruction QCP features criticality in both the spin and the charge (or single-particle) channels[22,52,53,63–65]. The significance of this physics for systems beyond heavy fermion metals is discussed later. More broadly, the Kondo destruction QCP is also captured by the evolution of entanglement entropy[53,66,67]; exploring entanglement properties, perhaps using emulating set-ups based on cold atoms or mesoscopic devices, will deepen our understanding of

this new type of quantum criticality and its associated strong correlation physics.

Unconventional superconductivity and other emergent phases. Quantum criticality provides a mechanism to soften the electronic system and nucleate new phases. A widely recognized case in point is the development of unconventional superconductivity[68,69]. In $CePd_2Si_2$, a dome of superconductivity is observed around a pressure-induced QCP[68]. This QCP was discussed as being of SDW type and the superconducting pairing was associated with antiferromagnetic paramagnons[70]. This led to the important question of whether a Kondo-destruction QCP can also promote superconductivity. Theoretical calculations suggest that this is indeed the case[71,72].

There are currently about 50 heavy fermion superconductors. Many of them seem to be driven by antiferromagnetic quantum criticality, but whether that is the case, and, if so, what the nature of the underlying QCP is, remains to be clarified in most cases. In $CeRhIn_5$, where a Kondo-destruction QCP was evidenced at a critical pressure from dHvA experiments performed above the upper critical field H_{c2} (REF.[4]), superconductivity did appear near that pressure[8,51], suggesting that it is driven by the Kondo destruction QCP. The optimal T_c is about 2.3 K (in zero field)[8,51], which is among the highest transition temperatures for 4*f*-electron-based heavy fermion superconductors.

$CeCu_2Si_2$ is the heavy fermion metal in which unconventional superconductivity was first discovered[73], with $T_c = 0.6$ K. The magnetic fluctuation spectrum changes noticeably on entering the superconducting state[74], an effect that was also studied in other heavy fermion superconductors[75]. This change in the fluctuation spectrum gives rise to a large gain in the magnetic exchange energy, which is about 20 times the superconducting condensation energy[74,76], thereby providing evidence that the quantum critical magnetic fluctuations are a major driving force for the development of unconventional superconductivity. It also implies a loss of kinetic energy of close to 20 times the superconducting condensation energy, which is compatible with pairing in the spin-singlet channel. As a result, the development of superconducting pairing weakens the Kondo-singlet correlation and thus transfers the *f*-electron spectral weight from low energies to above the Kondo-destruction energy scale $T^\star$ (REF.[76]). The precise form of the spin-singlet pairing order parameter has been reanalysed in recent years. A multi-orbital $d+d$ pairing[77,78] provides a natural understanding of the gap-like features that have recently been observed through measurements of the specific heat and superfluid stiffness at the lowest temperatures[79–81]. This pairing state obeys the prohibition of any onsite pairing amplitude by the Coulomb repulsion. It features a spin resonance in the superconducting state[74], and the correlation effect is expected to reduce its sensitivity to non-magnetic disorder[82]. The conventional *s*-wave pairing, which has also been invoked to explain the observed gap[80], involves electron overlap and thus costs too much Coulomb energy. Extended *s*-wave pairings have also been considered[83,84]. For the Fermi surface of $CeCu_2Si_2$, they are expected to be nodal, with any spin resonance being away from the intraband nesting wavevector observed experimentally[82]. Microscopically, the $d+d$ pairing order parameter, an irreducible representation of the crystalline point group, comprises intraband and interband *d*-wave pairing components. It is the non-commuting nature of the two components that produces a full gap on the Fermi surface, which is analogous to what happens in the ^{3}He superfluid B-phase[78].

For a long time, no superconductivity was found in $YbRh_2Si_2$. This changed when the specific heat and magnetization were measured at ultralow temperatures[85]. An analysis of the coupling between nuclear and electronic spins led to the picture that, below 2 mK, superconductivity coexists with hybrid nuclear–electron order, which reduces the primary electronic order and, consequently, enhances quantum critical fluctuations.

Other forms of emergent phases may also develop near a QCP. In $CeRhIn_5$ at ambient pressure, quantum oscillation and Hall effect measurements provided evidence for a Kondo destruction QCP near $B_0^\star \approx 30$ T (REF.[86]), which is considerably below the field for the zero-temperature magnetic to paramagnetic transition, $B_{c0} \approx 50$ T. Near $B_0^\star$, transport measurements in samples fabricated by focused ion beam milling have indicated the development of nematic correlations[87]. Whether static nematic order exists and, if so, whether it is nucleated by Kondo destruction quantum criticality are interesting questions that deserve further investigations.

New horizons for quantum phases

Many of the extensive developments on heavy fermion quantum criticality, reviewed above, correspond to the prototypical setting[28], in which the physics of the competition between Kondo and RKKY interaction in a (spin-1/2) Kondo lattice dominates. It is becoming increasingly clear that some of the most interesting phenomena, such as quantum criticality associated with electron localization and the formation of new phases, are not limited to this canonical case but can be generalized to much broader contexts, where other building blocks or interactions also play an important role (FIG. 6).

Frustration and dimensionality. The localization–delocalization transition discussed earlier originates from the different types of correlations that are promoted by the Kondo and RKKY interactions. The singlet formation among the spins in the antiferromagnetic state leads to a destruction of the static Kondo effect. When the degree of frustration *G* (REF.[88]) is large, spin singlets among the local moments develop even in a quantum paramagnet[15–17] and are detrimental to the formation of the Kondo entanglement. Incorporating this line of consideration into the Kondo physics leads to a global phase diagram[89–92], featuring both J_K (or $J_K N_F$; see Supplementary Box 1) and the frustration parameter *G* as non-thermal tuning parameters (FIG. 3c). At large values of *G*, when the Kondo coupling is not too large, the static Kondo singlet amplitude vanishes, and a paramagnetic phase with small Fermi surface, P_S, is stabilized,

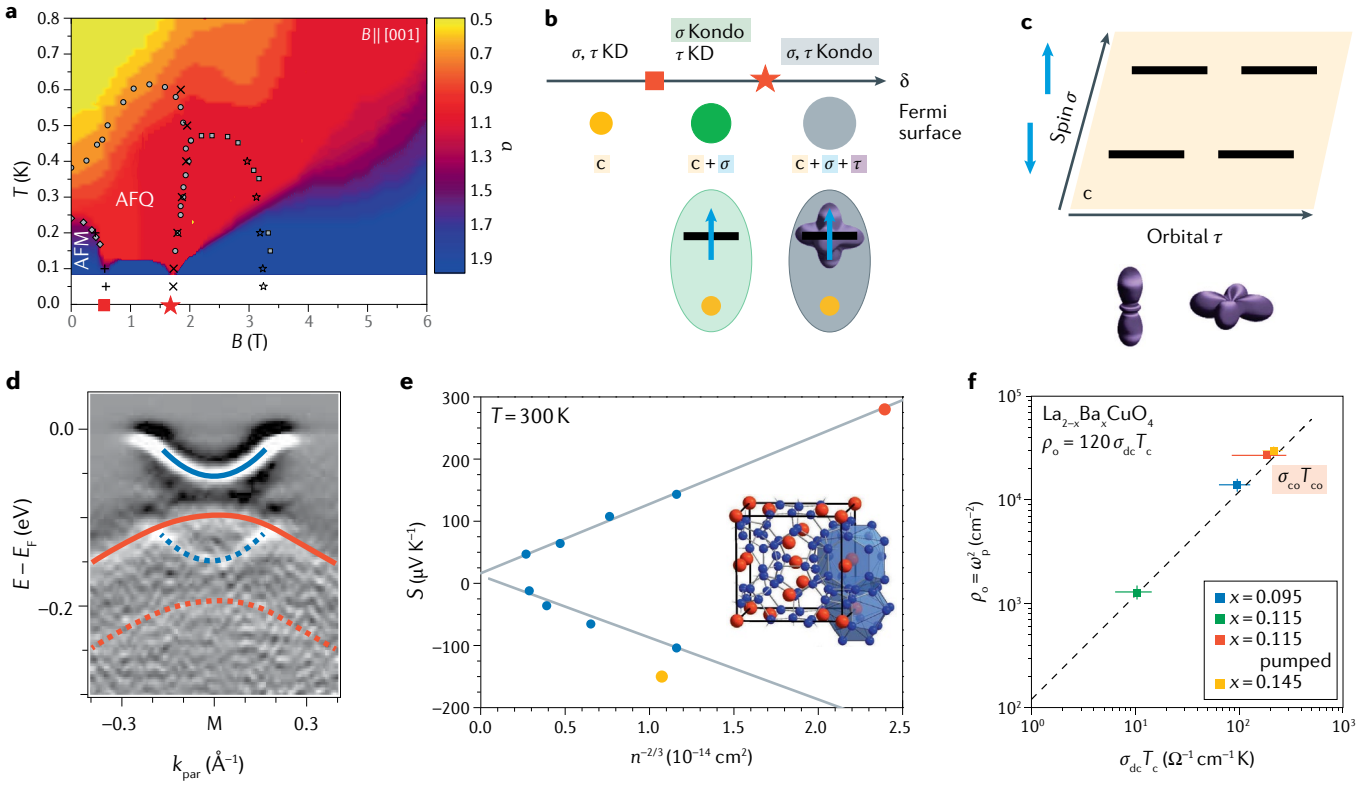

Fig. 6 | **Composite and boosted interactions. a** | Phase diagram of temperature versus tuning parameter for the heavy fermion compound $Ce_3Pd_{20}Si_6$, featuring phases of antiferromagnetic (AFM) and antiferroquadrupolar (AFQ) order that are suppressed at two consecutive quantum critical points (red square and red star), from which non-Fermi-liquid behaviour with a resistivity exponent α (colour bar) close to 1 emerges. **b** | Sketches visualizing the interaction of spin, σ, and orbital, τ, degrees of freedom with conduction electrons, c, in the form of two stages of Kondo destruction. **c** | Degrees of freedom that entangle in the Kondo phases of $Ce_3Pd_{20}Si_6$. **d** | Second energy derivative of angle resolved photoemission spectroscopy data of monolayer FeSe on $SrTiO_3$, revealing replicas (dashed guides-to-the-eye) of the main bands (full lines). k_{par} refers to momentum along the Γ–M direction. **e** | Thermopower, S, at 300 K of the type-I clathrate $Ce_{1.1}Ba_{6.9}Au_{5.5}Si_{40.5}$ (yellow symbol) compared with non-4f reference compounds (blue, red) of various charge-carrier concentrations n. The inset sketches the type-I clathrate crystal structure, with two molecular cages highlighted by blue shading. **f** | Superfluid density, ρ_0, versus product of zero-frequency conductivity σ_{dc} (measured just above the superconducting transition, T_c) and T_c, including what is interpreted as the transition temperature after pumping (red symbol, where σ_{co} is the conductivity just above the charge ordering temperature, T_{co}), for several dopings of $La_{2-x}Ba_xCuO_4$, providing an indication of light-boosted superconductivity. The error bars represent uncertainties in extracting the respective quantities from the experiments. Parts **a**, **b** and **c** are adapted with permission from REF.[14]. Part **b** is adapted with permission from REF.[14]. Part **d** is adapted with permission from REF.[168]. Part **e** is adapted with permission from REF.[117]. Part **f** is adapted with permission from REF.[173].

possibly in the form of a metallic spin liquid. Concrete theoretical studies of the global phase diagram in frustrated Kondo lattice models have been carried out, using a large-N method in the case of the Shastry–Sutherland lattice[93] and through a quantum Monte Carlo technique for a model on the honeycomb lattice[94].

To link such theoretical phase diagrams to experiments, one should be able to quantify the degree of frustration and, ideally, continuously vary it by some external tuning parameter. In insulating quantum magnets, the frustration strength can be quantified by the ratio of the paramagnetic Weiss temperature and the ordering temperature or, in a more sophisticated way, by modelling magnetic structure data to extract exchange interactions[95,96]. In heavy fermion systems, however, the local moment exchange interaction is typically dominated by the long-ranged RKKY interaction, and thus the conduction electrons and anisotropies in their densities of states at the Fermi level may also play an important role in defining the degree of frustration.

Yet, so far, frustration in heavy fermion systems has been discussed mostly in terms of the more intuitive concept of local moments situated on (partially) frustrated lattices[97–103]. Examples are $Pr_2Ir_2O_7$ with a pyrochlore lattice of Pr atoms[97,103], CeRhSn (REF.[100]) and CePdAl (REFS[99,102]) with Ce atoms located on distorted kagome planes, and $HoInCu_4$ with a face-centred cubic (fcc) lattice of the Ho atoms[104] (although the Kondo interaction in this latter low-carrier density system is likely to be negligible). In $Pr_2Ir_2O_7$, non-Fermi-liquid behaviour is observed above certain cutoffs in temperature and field (with the cutoffs possibly originating from spin freezing)[97,105]. The non-Fermi-liquid behaviour could be due to spin liquid behaviour or quantum criticality from a nearby magnetic QCP. In CeRhSn, thermodynamic properties show non-Fermi-liquid behaviour only within the frustrated plane[100], while it is suppressed under uniaxial pressure applied within the plane, which lifts the frustration[106]. These observations are interpreted as providing evidence for frustration-induced

SU(4) spin–orbital-coupled Kondo effect
Entwined spin and orbital building blocks form an SU(4) local multiplet, which is coupled to the corresponding conduction electron degrees of freedom to form an SU(4) Kondo singlet.

non-Fermi-liquid behaviour. In CePdAl, a region of non-Fermi-liquid behaviour was found in a pressure–magnetic field phase diagram[102] and associated with the P_S phase (FIG. 3c). Regions of non-Fermi-liquid behaviour are, however, also seen in heavy fermion metals without any obvious element of geometric frustration[107,108]. In $YbRh_2(Si_{1.95}Ge_{0.05})_2$, a P_S phase was shown to be nested between an AF_S phase and a P_L phase[108], thus directly confirming trajectory III in the theoretical phase diagram (FIG. 3c). Further work is needed to understand how this P_S phase relates to the ones hinted at in the above geometrically frustrated local moment systems with much weaker Kondo interaction. A recent scanning tunnelling microscopy study on $Pr_2Ir_2O_7$ provided evidence for a P_L to P_S transition through the tuning of minute disorder potential on the nanoscale[103].

A new platform for the exploration of this physics is provided by heavy fermion thin films. In insulating local moment systems, quantum fluctuations are not only boosted by (geometrical) frustration but also by reduced dimensionality (FIG. 3d). Thus, in the search for materials in which the *G* parameter can be (quasi-)continuously varied, systems with tunable dimensionality should also be considered[6]. High-quality thin films grown by molecular beam epitaxy[7,109,110] appear a promising way forward. Superlattices of heavy fermion metals with normal metals ($CeIn_3/LaIn_3$ and $CeRhIn_5/YbRhIn_5$) have indeed shown the emergence of non-Fermi-liquid signatures with decreasing superlattice period[109,110]. Whether this represented the appearance of the P_S phase (along trajectory III in FIG. 3c), or quantum criticality from the suppression of antiferromagnetic order (along trajectory I in FIG. 3c) is an interesting question for future studies. Particularly instructive would be investigations of superlattices with passive (non-metallic) spacer compounds. In the opposite direction, one can reduce *G* by going to the 3D limit. The cubic compound $Ce_3Pd_{20}Si_6$ fits this prescription. Magnetotransport and thermodynamic measurements have firmly established that the Kondo destruction appears within the ordered part of the phase diagram[6], thus representing an example of trajectory II in FIG. 3c.

Entwined degrees of freedom and hybrid interactions. We have so far considered the case of localized spins coupled to each other and to conduction electrons by spin-exchange interactions. The rich settings of condensed matter systems, however, allow us to use, or even design, alternative degrees of freedom. In heavy fermion systems, physics beyond the spin-only case comes in naturally. For the 4*f* (5*f*) electrons of the rare earth (actinide) elements, the intra-atomic spin–orbit coupling is large, and thus having effective moments of total angular momentum $J > 1/2$, which encompass both spins (dipoles) and higher multipolar moments, is the generic case. Crystal electric fields split these spin–orbit coupled states, but even the ground state will, in general, not be a spin-only Kramers doublet.

An example for such a multipolar Kondo system is the cubic heavy fermion compound $Ce_3Pd_{20}Si_6$. Its $Ce4f^1$ crystal-field-split ground state is a Γ_8 quartet, which has multipolar character. Surprisingly simple low-energy behaviour was observed for this case[14]. Across two QCPs, one at the border of antiferromagnetic (AFM), the other at the border of antiferroquadrupolar (AFQ) order (FIG. 6a), two distinct electron localization transitions take place, driven by a single degree of freedom at a time (FIG. 6b,c). They were understood as a sequential destruction of an SU(4) spin–orbital-coupled Kondo effect[14].

In other classes of strongly correlated electron systems there is also ample evidence for entwined degrees of freedom. In the manganites[11] and fullerides[111], it is also spin and orbital degrees of freedom that interplay, and in the iron pnictides and chalcogenides, more than one 3*d* orbital is important for the physics near the Fermi energy[12]. In the cuprates, charge order emerges and interplays with the spin degrees of freedom[1,112], and even in magic-angle bilayer graphene, the physics probably depends on both the spin and valley degrees of freedom[10]. To advance the understanding of the rich physical phenomena present in all these materials, it is important to decipher the roles that the different degrees of freedom play in determining the stable phases (Supplementary Fig. 1) and excitations associated with them, as well as with (quantum) phase transitions between them.

Strong electron interactions can also be modified by other interactions. In fact, the competition between the different energy scales associated with the various degrees of freedom — which also leads to the rich phase diagrams (Supplementary Fig. 1) — makes these systems generally highly responsive to all kinds of stimuli. Particularly interesting are situations where alternative interactions boost strong correlation effects, thereby enhancing functionality.

One way of boosting strong correlation effects is by using phonons. The interplay of the electron–electron Coulomb interaction and phonon-mediated electron interaction effects is captured by the Anderson–Holstein model[113], which has been much explored in the context of single molecular transistors[114,115]. In Kondo systems, increasing the coupling of the conduction electrons with local optical phonons was shown to enhance the Kondo temperature by orders of magnitude, up to a point beyond which the charge Kondo effect is stabilized[116]. The phonon-boosting mechanism was put forward to explain a high-temperature Kondo effect in a Ce-based thermoelectric rattler compound (which has an oversized space in the crystal structure for atoms to 'rattle')[117]. Its thermopower at room temperature was shown to be strongly enhanced over values found in a 4*f* moment-free reference compound (FIG. 6e) although the bare Kondo temperature of the system at low temperatures, where the optical phonon mode associated with the atoms rattling is not activated, was only 1 K. This effect almost doubled the thermoelectric figure of merit[117]. The strong response to phonons in this type-I clathrate compound is due to its special crystal structure, with an atom trapped in an oversized cage. Whereas most heavy fermion compounds lack such special structures and are much less sensitive to phonons, other strongly correlated electron systems, in particular with polar bonds and/or reduced dimensionality, do show phonon- (and photon-) boosting effects.

Correlation-driven topology. With the advent of topological theories in electronic materials[21,118–123] the question of how strong correlations and topology may interplay is attracting much interest. Here we focus on Weyl semimetals[121–123] (see Supplementary Box 2).

Theoretical predictions for non-interacting electron systems are becoming ever more efficient in guiding the search for new candidate materials. In principle, topological invariants — key quantities in defining the topological nature of the electrons' wavefunctions — can be directly calculated from electronic band structure. Because this is a laborious process, other, higher-throughput methods were also developed. These classify materials by certain indicators for topology, most notably symmetry eigenvalues[124–128].

Although — or even because — these approaches have by now identified enormous numbers of candidate materials, clear-cut experimental confirmations remain a formidable task. ARPES is playing a central role in this (see panels a–d in Supplementary Box 2), even though the interpretation of ARPES data is not always easy. First, to disentangle surface from bulk and topological from topologically trivial states, comparison is needed with ab initio calculations, which are challenging for real surfaces even in the non-interacting case. Second, the rather intense incident light needed for ARPES may dope the surface and thus modify the band structure[129]. Complementary experimental techniques, including (magneto)transport, optical spectroscopy and quantum oscillation experiments, are thus equally important and have indeed provided independent evidence[123,130–133].

To address the effect of correlations, theoretical treatments can either study how electron correlations modify (known) non-interacting topological states, or explore how non-trivial topology can be introduced into (known) strongly correlated electronic states. A recent example in the spirit of the first approach is an optical spectroscopy study of the nodal-line semimetal ZrSiSe (REF.[134]), where a comparison with density functional theory (DFT) revealed a reduction of the Fermi velocity with respect to the non-interacting one derived by DFT by almost 30%, an effect that was attributed to interactions (FIG. 2d). Similar effects are seen in several other topological semimetals (FIG. 2e). In graphene, a quantum Monte Carlo study showed short- and long-range Coulomb interaction effects to reduce the Fermi velocity by about 40% near the strong-coupling fixed point[135].

For the case of Schrödinger particles, even Fermi liquids with orders-of-magnitude renormalizations (FIG. 2a) may — but do not have to (FIG. 2b,c) — be adiabatically connected to the non-interacting state. Such a situation could also apply to Dirac particles. Thus, exploring how non-trivial topology affects strongly correlated electron states may well discover phenomena that have no analogues in the non-interacting world, a particularly exciting prospect.

A promising setting to find such entirely new electronic phases is systems where strong electron correlations and large spin–orbit interaction coexist, as is the case in heavy fermion compounds. To single out the effect of the spin–orbit interaction, a strategy to selectively tune its strength should be identified. This attempt was made in a chemical substitution study of the Kondo insulator $Ce_3Bi_4Pt_3$ in which the 5*d* element Pt was successively replaced by the 4*d* element Pd (REF.[18]). As this substitution is isostructural, isoelectronic and essentially isosize, the large mass difference between Pt and Pd and the associated difference in atomic spin–orbit coupling strength was suggested to play the dominant role in the tuning[18]. A transformation from an insulator to a semimetal was observed with increasing Pd content, with the end compound $Ce_3Bi_4Pd_3$ showing striking signatures of non-trivial topology. The low-temperature electronic specific heat coefficient $\Delta C/T$ is linear in T^2 (FIG. 7a), pointing to a linear electronic dispersion in momentum space, as expected for Dirac or Weyl fermions. The velocity of the corresponding fermions calculated from the slope Γ is less than 1,000 m s^{-1}, which is three orders of magnitude lower than a typical Fermi velocity of simple metals. Because this unusual specific heat contribution appeared only below the Kondo temperature — which is 1/1,000 of the typical Fermi temperature — it was argued to be Kondo-driven[18].

Indeed, a theoretical study of the periodic Anderson model on a non-centrosymmetric lattice discovered a Kondo-driven topological semimetal phase, dubbed Weyl–Kondo semimetal[19], with extremely flat linear dispersion around Weyl nodes pinned to the Fermi energy (FIG. 7b,c), in agreement with the above experiments[18].

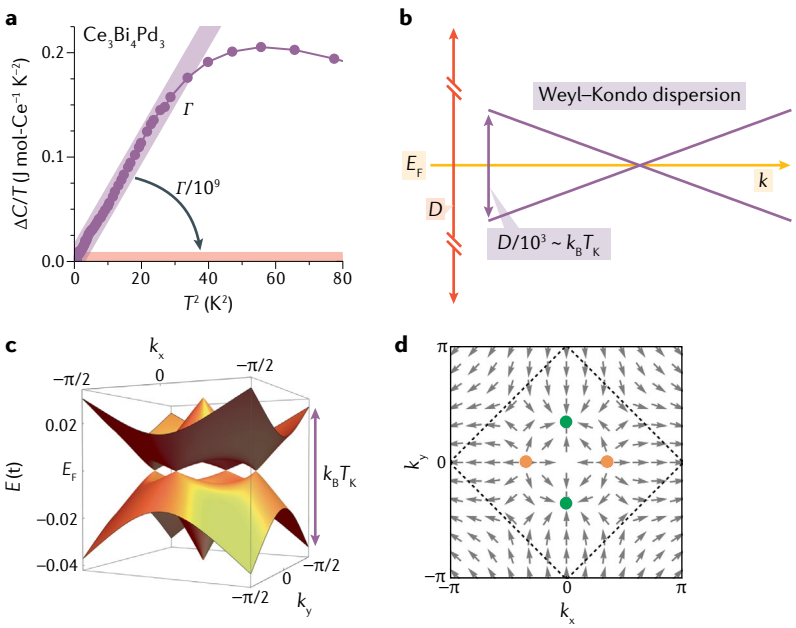

Fig. 7 | **Weyl–Kondo semimetals. a** | Electronic specific heat coefficient $\Delta C/T$ of $Ce_3Bi_4Pd_3$, displaying linear-in-T^2 behaviour at low temperatures. Slope, Γ. **b** | Sketch of the linear electronic dispersion in momentum space near a Weyl point and the band renormalization — from the underlying non-interacting bandwidth D to the width k_BT_K dictated by the Kondo interaction — corresponding to the specific heat result. **c** | Dispersion of a theoretical model for a Weyl–Kondo semimetal. The energy E is given in units of the nearest-neighbour term t of the bare conduction-electron hopping parameters. **d** | Berry curvature field (with grey arrows indicating its direction) near the Weyl and anti-Weyl nodes (orange and green dots, respectively) for the same model. Part **a** is adapted with permission from REF.[18]. Parts **c** and **d** are adapted with permission from REF.[19].

Berry curvature
The gauge-invariant rank-two tensor that is associated with the Berry (or geometric) phase; for itinerant electrons, it acts as a fictitious magnetic field in momentum space and is singularly large around the nodes of a Weyl semimetal.

The Kondo effect cooperates with the non-symmorphic space group of the underlying lattice, not only to generate the strongly renormalized Weyl nodes but also to place them at the Fermi energy[136]. Weyl and anti-Weyl nodes are sources and sinks of Berry curvature (FIG. 7d). Recent experiments have directly evidenced these Weyl nodes via spontaneous (zero magnetic field) Hall effect measurements[137] and even seen them annihilate in large magnetic fields[138]. The giant magnitude of the spontaneous Hall effect, and its electric field and frequency dependence, were understood as the Weyl nodes being part of the Kondo resonance, situated in immediate proximity to the Fermi energy[137]. The calculations[19] also predicted surface states that feature strongly renormalized Fermi arcs, which still await experimental confirmation.

Weyl physics is being explored also in other Ce- and Yb-based intermetallic compounds[139–141], creating the exciting opportunity to discover signatures of strong correlation-driven electronic topology there too. Together with theoretical efforts[136,142–150], this may help to establish the new field of strongly correlated electronic topology.

Organizing principles across materials platforms

We have highlighted how the heavy fermion systems provide a setting to search for and explore quantum criticality and new quantum phases. Ultimately, the field of strongly correlated electron systems aims to develop the organizing principles that may operate across the materials platforms. With that consideration in mind, we discuss how the insights gained from the heavy fermion field affect other classes of strongly correlated systems and beyond (FIG. 8).

Quantum criticality and electronic localization–delocalization. In heavy fermion quantum criticality, the physics of Kondo destruction plays an essential role (FIG. 8a,b). From the critical phenomenon perspective, the Kondo-destruction QCP involves critical physics that is beyond the Landau framework of order parameter fluctuations. The destruction of the static Kondo effect gives rise to critical modes that are in addition to the slow fluctuations of the antiferromagnetic order parameter. From the correlated electron perspective, this type of QCP epitomizes metallic quantum criticality in which the suppression of electronic orders entwines with an electronic localization–delocalization transition[2–7] (FIG. 8a). Such a transition of electrons in a metallic background, and its accompanying jump of Fermi surface, have also been discussed in the context of hole-doped high-T_c cuprates. A pronounced change of the Hall coefficient as function of hole doping, measured in high magnetic fields to suppress superconductivity, is evidence for a change of Fermi surface (FIG. 8c)[1]. Important questions for future studies remain: whether the gradual crossover seen at 50 K extrapolates, in the $T = 0$ limit, to a sharp jump (with zero crossover width) as seen in heavy fermion metals across Kondo-destruction QCPs[3,5,6] and whether the position of this (putative) Fermi surface jump coincides with a QCP at optimal doping. An indication for quantum criticality underlying this Fermi surface change comes from quantum oscillation experiments that reveal an (almost three-fold) increase of the effective mass towards optimum doping[112] (FIG. 8d). Again, this behaviour is reminiscent of the (more marked; see FIG. 2b,c) effective mass enhancements observed upon approaching Kondo-destruction QCPs in heavy fermion compounds.

This experimental analogy extends to the domain of theoretical analyses. In heavy fermion systems, the destruction of the static Kondo effect and the associated jump of the Fermi surface have been extensively analysed using the extended dynamical mean-field theory (EDMFT) approach to the Kondo lattice model[22,52,53]. A similar method has recently been adopted to describe the localization–delocalization transition in the single-band Hubbard model in the context of the high-T_c cuprates[151,152].

The global phase diagram of heavy fermion systems (FIG. 8a) delineates whether a jump of Fermi surface is concurrent with or detached from the suppression of antiferromagnetic or other electronic orders. For instance, in the presence of strong frustration, a metallic spin liquid phase may occur, as tentatively evidenced in the geometrically frustrated compound CePdAl (FIG. 8b). Also in the case of high-T_c cuprates, the relationship between a sudden reconstruction of the Fermi surface and the development of electronic orders at zero temperature is a central issue.

Additionally, the localization–delocalization transition comes into play near the Mott transition in Mott–Hubbard systems, as has been considered theoretically[153,154]. Organic charge-transfer salts have provided a versatile materials setting to study this issue. For example, measurements of the Hall coefficient in a doped organic superconductor, κ-$ET_4Hg_{2.89}Br_8$, have hinted at a striking transformation of the Fermi surface[9]. In intermetallic systems, there has been considerable recent development on materials with a potential spin-liquid ground state. Pressurizing such compounds presents a promising new setting to realize a Mott transition and elucidate the accompanying evolution of the Fermi surface. Progress along this direction has recently been reported in a high-pressure study of $NaYbSe_2$ (FIG. 8e)[155].

The Kondo-destruction QCP, with the localization–delocalization transition of the *f* electrons in a metallic background[22,23,156], represents the earliest example of orbital-selective Mott transitions. In *d*-electron systems, this transition was first discussed in the context of the ruthenates[157]. Unlike in the heavy fermion case, the analysis was done in the band basis; different bands, by definition, do not hybridize with each other. In reality, the Coulomb interactions are expressed in the orbital basis, and crystalline symmetry generically allows for inter-orbital kinetic coupling. In that sense, the orbital-selective Mott transition in *d*-electron systems shares one important aspect with what happens in the heavy fermion compounds: the realization of the orbital-selective Mott phase requires that the electron correlations suppress the inter-orbital hybridization. This has been stressed in the context of iron-based superconductors[158].

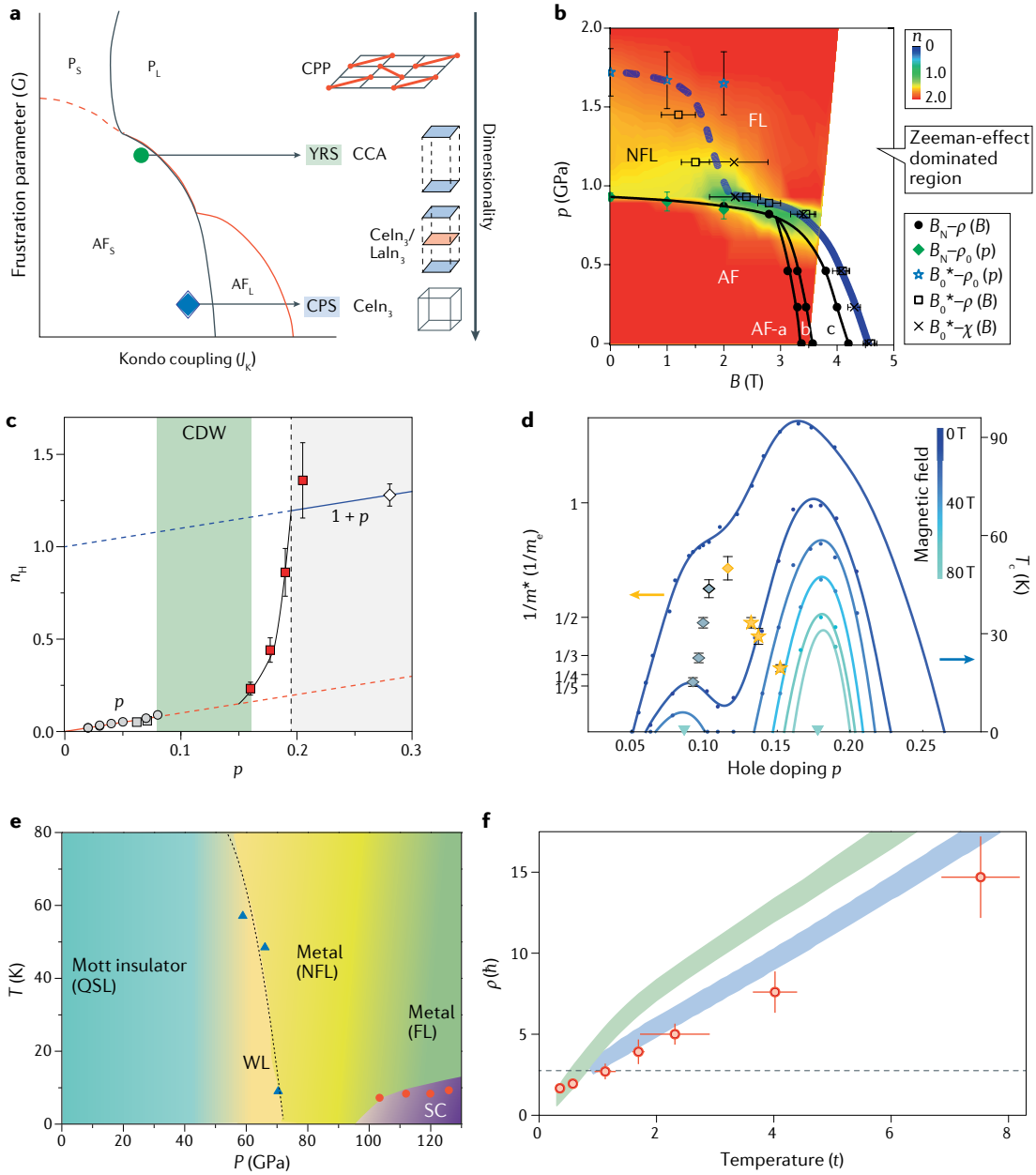

Fig. 8 | **Electronic localization–delocalization and bad metal behaviour in correlated quantum matter. a** | Schematic zero-temperature phase diagram with axes of Kondo coupling J_K and frustration parameter G. P and AF stand for paramagnetic and antiferromagnetic phases, while the subscripts L and S denote large and small Fermi surface. Quantum phase transitions of Kondo destruction type are denoted by the black line. Dimensionality (right) helps to calibrate the placement of selected materials (CPS, $Ce_3Pd_{20}Si_6$; YRS, $YbRh_2Si_2$; CCA, $CeCu_{6-x}Au_x$; CPP, Ce_2Pt_2Pb). **b** | Pressure–magnetic field phase diagram of CePdAl, extrapolated from finite-temperature results to $T = 0$. B_N denotes antiferromagnetic phase boundaries, B_0^* an anomaly in the data interpreted as partial delocalization of the 4*f* states. The colour code represents n in $\Delta\rho \sim AT^n$, revealing a range of non-Fermi-liquid (NFL) behaviour. **c** | Doping, p, dependence of the Hall number, n_H, in the normal state (reached by application of large magnetic fields) for $La_{2-x}Sr_xCuO_4$ (circles), $YBa_2Cu_3O_{6+\delta}$ (grey and red squares) and strongly overdoped $Tl_2Ba_2CuO_{6+\delta}$ (white diamond). **d** | Inverse effective mass (yellow and grey symbols, from quantum oscillations) and T_c (blue circles, from resistivity, at magnetic fields indicated by the blue colour code) versus hole doping in $YBa_2Cu_3O_{6+\delta}$. **e** | Temperature–pressure phase diagram of $NaYbSe_2$ with regions featuring quantum spin liquid (QSL), weak localization (WL), non-Fermi-liquid (NFL), superconducting (SC) and Fermi liquid (FL) behaviour. **f** | Resistivity versus temperature of ultracold lithium-6 atoms in a 2D optical lattice, from experiment (red points), finite-temperature Lanczos calculations (blue) and single-site dynamical mean-field theory (DMFT) (green); the dashed line represents the upper bound on Drude resistivity. Here, temperature is measured in terms of $t = 925$ Hz, the tunnelling rate between two nearest-neighbour sites on a square optical lattice. Part **a** is adapted with permission from REF.[6]. Part **b** is adapted with permission from REF.[102]. Part **c** is adapted with permission from REF.[1]. Part **d** is adapted with permission from REF.[112]. Part **e** is adapted with permission from REF.[155]. Part **f** is adapted with permission from REF.[175].

'Flat' bands and electron correlations. In heavy fermion systems, the *f* electrons experience a large local Coulomb interaction U (including the Hubbard and Hund's coupling) and, in addition, their bare bandwidth W_f is small. The enhanced U/W_f is responsible for the strongly correlated nature of the *f*-electron system.

In *d*-electron systems, one may be able to use the crystalline lattice geometry to create destructive interference of electron propagation and produce narrow bands and, thus, to engineer enhanced correlation effect. In recent years, this direction has been explored in a number of materials, including several Fe-based kagome-lattice materials[159,160]. Although the focus has been on the identification of Weyl nodes in their magnetically ordered states, one can envisage the 'flat' bands providing a setting for strong correlation physics that may bear some analogy with what has been so extensively studied in heavy fermion metals.

Beyond the standard correlated electron cases, twisted bilayer graphene has provided a synthetic setting for narrow bands and strong correlation physics. When two layers of graphene are twisted to special angles[161], moiré bands are formed with a small bandwidth W_m. Even though the *p* electrons have relatively small Coulomb repulsion, which is smaller still due to the spatially extended nature of the electronic states in the moiré bands, U/W_m can be greatly enhanced compared with their bare graphene counterpart. In practice, U/W_m in the 'magic-angle' twisted bilayer graphene is of order unity. The emergence of a dome of superconductivity[10,162,163], nematic correlations[164–166] and other phenomena establish these systems as a new playground to explore strong correlation physics. The intertwining of correlations and topology adds a further layer of richness to the physics of these systems.

Strong electron correlations boosted by other interactions. As discussed earlier for the heavy fermion case, strong correlations also create sensitivity to other interactions. For instance, phonon-boosting effects have been suggested for a number of unconventional superconductors. In FeSe, a large enhancement of the superconducting gap-opening temperature — from 8 K in bulk FeSe to nearly 70 K when a single-unit-cell FeSe layer is grown on $SrTiO_3$ (REF.[167]) — was attributed in part to the coupling of electrons in FeSe to a phonon mode in $SrTiO_3$. This proposal has received support from the appearance of strong replica bands (FIG. 6d)[168] and has triggered further work. For instance, recent theoretical work has suggested that the small-momentum electron–phonon interaction underlying the replica bands boosts but cannot trigger superconductivity in this system[169]. Whether phonons also boost superconductivity in other 2D systems is a topic of active debate[170].

Photons may also enhance electron interactions, an effect investigated in ultrafast pump–probe experiments with intense light pulses in different frequency ranges[171]. Such experiments have demonstrated transitions between (transient) phases, for instance insulator–metal or metal–superconductor transitions. Pioneering work on light-induced superconductivity on the non-superconducting stripe-ordered cuprate $La_{1.675}Eu_{0.2}Sr_{0.125}CuO_4$ revealed transiently enhanced interlayer tunnelling only 1–2 ps after irradiation with an intense mid-infrared femtosecond pulse[172]. Very recently, evidence for metastable light-induced superconductivity was found, again in a stripe-ordered cuprate $La_{1.885}Ba_{0.115}CuO_4$ (FIG. 6f)[173] but also in K_3C_{60} (REF.[174]). In the former, the effect was attributed to the melting of the stripe order, delocalizing halted electrons that then form Cooper pairs. In the latter, where the pump photon energy was at least one order of magnitude larger than the low-temperature equilibrium superconducting gap, coupling of light with high-energy excitations, either molecular vibrations or collective electronic modes, was suggested.

Strong correlations and topological states. We have highlighted how heavy fermion metals display a rich variety of quantum phases. A tip of an iceberg is now seen in metallic phases that are topological, particularly the Weyl–Kondo semimetal. The appearance of topological semimetals raises an intriguing question — how does electronic topology enrich strongly correlated electron physics? For example, do strongly correlated topological semimetals lead to new varieties of superconductors?

Conversely, the development of the Weyl–Kondo semimetal phase illustrates how strong correlations drive topological states. In realizing this phase, the Kondo effect cooperates not only with the spin–orbit coupling but also with the non-symmorphic space group. This points to a general strategy, namely that strong correlations cooperate with space-group symmetry in producing correlated topological states of matter. We expect much exploration to take place on this strategy in heavy fermion metals and in a variety of other strongly correlated electron systems.

Wider contexts. Strongly correlated systems display amplified responses to external stimuli. A defining property of heavy fermion metals is the large effective mass of their charge carriers, which is typically enhanced from the non-interacting value by three orders of magnitude. The amplification occurs in response to external parameters such as magnetic field, pressure or doping. For Weyl–Kondo semimetals, we have mentioned the giant responses of both thermodynamic and magnetotransport properties. This illustrates the extreme sensitivity that characterizes strongly correlated states of matter, which may be important for applications in quantum technology.

Finally, it is instructive to place the study of strongly correlated systems in the overall context of research in quantum materials and beyond. In quantum materials we let nature work for us and reveal new physics that might not have been conceived by our imagination. The corresponding models and concepts could then be studied in various contexts, for example ultracold atoms[175], photonic systems[176] or gravity. For example, cold atom systems can be used to emulate bad metals and strange metals (FIG. 8f). The emulated states can then be used for measurements that are challenging to perform in quantum materials. A case in point is quantum entanglement properties, which are easier to measure in cold atom systems[177].

Outlook

We have surveyed the considerable developments in quantum phases and fluctuations produced by strong correlations, using heavy fermion metals as a platform. The focus has been on the particularly interesting situation where quantum criticality — frequently seen in these systems at the border of antiferromagnetic order — involves quantum fluctuations that go beyond the suppression of the Landau order parameter, in the form of a destruction of the static Kondo effect. Because the Kondo effect involves charge and spin, breaking it up not only creates local moments that can order but also entails an electron localization–delocalization transition. The associated quantum critical behaviour continues to reveal new surprises, including dynamical scaling in the charge channel. Even though these systems are metallic, the presence of local moments allows for frustration and dimensionality as new axes of tuning. Experiments have thus probed a considerable phase space, and the understanding of the discovered phases and fluctuations is guided by theoretical work on the global phase diagram. There has been considerable new development in this delineation, from the realization of a frustration-induced strange metal phase to the sequential localization–delocalization from entwined spin and orbital degrees of freedom.

Quantum critical fluctuations turn the electronic system soft, and may therefore nucleate new phases, with unconventional superconductivity as prime example. There has been much excitement about how the electronic localization–delocalization transition and the associated notable Fermi surface transformation influences unconventional superconductivity. More generally, in the realm of emergent phases of metallic systems, recent studies seem to have seen the tip of the iceberg in how strong correlations drive topological phases.

These developments set the stage for answering a set of fascinating outstanding questions that are pertinent to strongly correlated metals beyond the heavy fermion settings. We close the Review by listing a few of them:

- How relevant is the electronic localization–delocalization transition to strongly correlated electron systems in general? For instance, how can we establish that the Fermi surface transformation observed in the high-T_c cuprates and other Mott–Hubbard systems reflects the amplified quantum fluctuations associated with electrons on the verge of localization? What are the pertinent tuning axes for an overall zero-temperature phase diagram that delineates the concurrence or detachment between the localization–delocalization transition and the development of electronic orders?
- We have hypothesized a strategy for strong correlations to produce topological states. In addition to the heavy fermion semimetals, what are the materials platforms that can be used to explore this strategy? Can an overall phase diagram be devised that delineates strong-correlation-driven topological phases and classifies their fluctuations?
- The rich phenomena observed in strongly correlated materials comes with considerable complexity. When disentangled, it leads to new and much clearer understanding. How can synthetic platforms such as cold atom or mesoscopic systems be most efficiently used to elucidate the underlying simplicity?
- We have pointed out the extreme sensitivity of strongly correlated systems to external stimuli and their giant responses, in particular if non-trivial topology is involved. Can this be exploited for new robust quantum devices, for applications such as quantum sensing or quantum computing?

Published online 22 December 2020

1. Badoux, S. et al. Change of carrier density at the pseudogap critical point of a cuprate superconductor. *Nature* **531**, 210–214 (2016).
2. Schröder, A. et al. Onset of antiferromagnetism in heavy-fermion metals. *Nature* **407**, 351–355 (2000).
3. Paschen, S. et al. Hall-effect evolution across a heavy-fermion quantum critical point. *Nature* **432**, 881–885 (2004).
4. Shishido, H., Settai, R., Harima, H. & Onuki, Y. A drastic change of the Fermi surface at a critical pressure in $CeRhIn_5$: dHvA study under pressure. *J. Phys. Soc. Jpn* **74**, 1103–1106 (2005).
5. Friedemann, S. et al. Fermi-surface collapse and dynamical scaling near a quantum-critical point. *Proc. Natl Acad. Sci. USA* **107**, 14547–14551 (2010).
6. Custers, J. et al. Destruction of the Kondo effect in the cubic heavy-fermion compound $Ce_3Pd_{20}Si_6$. *Nat. Mater.* **11**, 189–194 (2012).
7. Prochaska, L. et al. Singular charge fluctuations at a magnetic quantum critical point. *Science* **367**, 285–288 (2020).
8. Park, T. et al. Hidden magnetism and quantum criticality in the heavy fermion superconductor $CeRhIn_5$. *Nature* **440**, 65–68 (2006).
9. Oike, H., Miyagawa, K., Taniguchi, H. & Kanoda, K. Pressure-induced Mott transition in an organic superconductor with a finite doping level. *Phys. Rev. Lett.* **114**, 067002 (2015).
10. Cao, Y. et al. Unconventional superconductivity in magic-angle graphene superlattices. *Nature* **556**, 43–50 (2018).
11. Tokura, Y. & Nagaosa, N. Orbital physics in transition-metal oxides. *Science* **288**, 462–468 (2000).
12. Si, Q., Yu, R. & Abrahams, E. High-temperature superconductivity in iron pnictides and chalcogenides. *Nat. Rev. Mater.* **1**, 16017 (2016).
13. Kung, H.-H. et al. Analogy between the 'hidden order' and the orbital antiferromagnetism in $URu_{2-x}Fe_xSi_2$. *Phys. Rev. Lett.* **117**, 227601 (2016).
14. Martelli, V. et al. Sequential localization of a complex electron fluid. *Proc. Natl Acad. Sci. USA* **116**, 17701–17706 (2019).
15. Schaffer, R., Lee, E. K.-H., Yang, B.-J. & Kim, Y. B. Recent progress on correlated electron systems with strong spin-orbit coupling. *Rep. Prog. Phys.* **79**, 094504 (2016).
16. Savary, L. & Balents, L. Quantum spin liquids: a review. *Rep. Prog. Phys.* **80**, 016502 (2017).
17. Zhou, Y., Kanoda, K. & Ng, T.-K. Quantum spin liquid states. *Rev. Mod. Phys.* **89**, 025003 (2017).
18. Dzsaber, S. Kondo insulator to semimetal transformation tuned by spin–orbit coupling. *Phys. Rev. Lett.* **118**, 246601 (2017).
19. Lai, H.-H., Grefe, S. E., Paschen, S. & Si, Q. Weyl–Kondo semimetal in heavy-fermion systems. *Proc. Natl Acad. Sci. USA.* **115**, 93–97 (2018).
20. Stormer, H. L. Nobel lecture: The fractional quantum Hall effect. *Rev. Mod. Phys.* **71**, 875–889 (1999).
21. Wen, X.-G. Colloquium: Zoo of quantum-topological phases of matter. *Rev. Mod. Phys.* **89**, 041004 (2017).
22. Si, Q., Rabello, S., Ingersent, K. & Smith, J. Locally critical quantum phase transitions in strongly correlated metals. *Nature* **413**, 804–808 (2001).
23. Coleman, P., Pépin, C., Si, Q. & Ramazashvili, R. How do Fermi liquids get heavy and die? *J. Phys. Condens. Matter* **13**, R723–R738 (2001).
24. Senthil, T., Vojta, M. & Sachdev, S. Weak magnetism and non-Fermi liquids near heavy-fermion critical points. *Phys. Rev. B* **69**, 035111 (2004).
25. Keimer, B., Kivelson, S. A., Norman, M. R., Uchida, S. & Zaanen, J. From quantum matter to high-temperature superconductivity in copper oxides. *Nature* **518**, 179–186 (2015).
26. Si, Q. & Steglich, F. Heavy fermions and quantum phase transitions. *Science* **329**, 1161–1166 (2010).
27. Hewson, A. C *The Kondo Problem to Heavy Fermions* (Cambridge Univ. Press, 1997).
28. Doniach, S. The Kondo lattice and weak antiferromagnetism. *Physica B+C* **91**, 231–234 (1977).
29. Stewart, G. R. Non-Fermi-liquid behavior in *d*- and *f*-electron metals. *Rev. Mod. Phys.* **73**, 797–855 (2001).
30. Coleman, P. & Schofield, A. J. Quantum criticality. *Nature* **433**, 226–229 (2005).
31. v. Löhneysen, H., Rosch, A., Vojta, M. & Wölfle, P. Fermi-liquid instabilities at magnetic quantum critical points. *Rev. Mod. Phys.* **79**, 1015–1075 (2007).
32. Special Issue: Quantum criticality and novel phases. *Phys. Status Solidi B* **250**, 417–659 (2013).
33. Si, Q. & Paschen, S. Quantum phase transitions in heavy fermion metals and Kondo insulators. *Phys. Status Solidi B* **250**, 425–438 (2013).
34. Kirchner, S. et al. Colloquium: Heavy-electron quantum criticality and single-particle spectroscopy. *Rev. Mod. Phys.* **92**, 011002 (2020).
35. Andres, K., Graebner, J. E. & Ott, H. R. 4*f*-virtual-bound-state formation in $CeAl_3$ at low temperatures. *Phys. Rev. Lett.* **35**, 1779–1782 (1975).

36. Kadowaki, K. & Woods, S. B. Universal relationship of the resistivity and specific heat in heavy-fermion compounds. *Solid State Commun.* **58**, 507–509 (1986).
37. Tsujii, N., Kontani, H. & Yoshimura, K. Universality in heavy fermion systems with general degeneracy. *Phys. Rev. Lett.* **94**, 057201 (2005).
38. Jacko, A. C., Fjaerestad, J. O. & Powell, B. J. A unified explanation of the Kadowaki–Woods ratio in strongly correlated metals. *Nat. Phys.* **5**, 422–425 (2009).
39. Zhu, L., Garst, M., Rosch, A. & Si, Q. Universally diverging Grüneisen parameter and the magnetocaloric effect close to quantum critical points. *Phys. Rev. Lett.* **91**, 066404 (2003).
40. Wu, J., Zhu, L. & Si, Q. Entropy accumulation near quantum critical points: effects beyond hyperscaling. *J. Phys. Conf. Ser.* **273**, 012019 (2011).
41. Keimer, B. & Moore, J. E. The physics of quantum materials. *Nat. Phys.* **13**, 1045 (2017).
42. Ball, P. Quantum materials: where many paths meet. *MRS Bull.* **42**, 698–705 (2017).
43. Hussey, N. E., Takenaka, K. & Takagi, H. Universality of the Mott–Ioffe–Regel limit in metals. *Phil. Mag.* **84**, 2847–2864 (2004).
44. Yi, M., Zhang, Y., Shen, Z.-X. & Lu, D. Role of the orbital degree of freedom in iron-based superconductors. *npj Quantum Mater.* **2**, 57 (2017).
45. Dressel, M. et al. Correlation gap in the heavy-fermion antiferromagnet UPd_2Al_3. *Phys. Rev. B* **66**, 035110 (2002).
46. Qazilbash, M. M. et al. Electronic correlations in the iron pnictides. *Nat. Phys.* **5**, 647–650 (2009).
47. Yamamoto, S. & Si, Q. Fermi surface and antiferromagnetism in the Kondo lattice: an asymptotically exact solution in $d>1$ dimensions. *Phys. Rev. Lett.* **99**, 016401 (2007).
48. Gegenwart, P. et al. Multiple energy scales at a quantum critical point. *Science* **315**, 969–971 (2007).
49. Seiro, S. et al. Evolution of the Kondo lattice and non-Fermi liquid excitations in a heavy-fermion metal. *Nat. Commun.* **9**, 3324 (2018).
50. Hegger, H. et al. Pressure-induced superconductivity in quasi-2D $CeRhIn_5$. *Phys. Rev. Lett.* **84**, 4986–4989 (2000).
51. Knebel, G., Aoki, D., Brison, J.-P. & Flouquet, J. The quantum critical point in $CeRhIn_5$: a resistivity study. *J. Phys. Soc. Jpn* **77**, 114704–114717 (2008).
52. Grempel, D. R. & Si, Q. Locally critical point in an anisotropic Kondo lattice. *Phys. Rev. Lett.* **91**, 026401 (2003).
53. Hu, H., Cai, A. & Si, Q. Quantum criticality and dynamical Kondo effect in an SU(2) Anderson lattice model. Preprint at https://arxiv.org/abs/2004.04679 (2020).
54. Matsumoto, Y. Quantum criticality without tuning in the mixed valence compound β-$YbAlB_4$. *Science* **331**, 316–319 (2011).
55. Hertz, J. A. Quantum critical phenomena. *Phys. Rev. B* **14**, 1165–1184 (1976).
56. Millis, A. J. Effect of a nonzero temperature on quantum critical points in itinerant fermion systems. *Phys. Rev. B* **48**, 7183–7196 (1993).
57. Moriya, T.*Spin Fluctuations in Itinerant Electron Magnetism* Vol. 56, 44–81 (Springer, 1985).
58. Levin, K. & Valls, O. Phenomenological theories of liquid ^{3}He. *Phys. Rep.* **98**, 1–56 (1983).
59. Cai, A., Hu, H., Ingersent, K., Paschen, S. & Si, Q. Dynamical Kondo effect and Kondo destruction in effective models for quantum critical heavy fermion metals. Preprint at https://arxiv.org/abs/1904.11471 (2019).
60. Nejati, A., Ballmann, K. & Kroha, J. Kondo destruction in RKKY-coupled Kondo lattice and multi-impurity systems. *Phys. Rev. Lett.* **118**, 117204 (2017).
61. Arndt, J. Spin fluctuations in normal state $CeCu_2Si_2$ on approaching the quantum critical point. *Phys. Rev. Lett.* **106**, 246401 (2011).
62. Senthil, T., Vishwanath, A., Balents, L., Sachdev, S. & Fisher, M. Deconfined quantum critical points. *Science* **303**, 1490–1494 (2004).
63. Zhu, L., Kirchner, S., Si, Q. & Georges, A. Quantum critical properties of the Bose–Fermi Kondo model in a large-*N* limit. *Phys. Rev. Lett.* **93**, 267201 (2004).
64. Komijani, Y. & Coleman, P. Emergent critical charge fluctuations at the Kondo breakdown of heavy fermions. *Phys. Rev. Lett.* **122**, 217001 (2019).
65. Cai, A., Yu, Z., Hu, H., Kirchner, S. & Si, Q. Dynamical scaling of charge and spin responses at a Kondo destruction quantum critical point. *Phys. Rev. Lett.* **124**, 027205 (2020).
66. Pixley, J. H. et al. Entanglement entropy near Kondo-destruction quantum critical points. *Phys. Rev. B* **91**, 245122 (2015).
67. Wagner, C., Chowdhury, T., Pixley, J. H. & Ingersent, K. Long-range entanglement near a Kondo-destruction quantum critical point. *Phys. Rev. Lett.* **121**, 147602 (2018).
68. Mathur, N. et al. Magnetically mediated superconductivity in heavy fermion compounds. *Nature* **394**, 39–43 (1998).
69. Steglich, F. & Wirth, S. Foundations of heavy-fermion superconductivity: lattice Kondo effect and Mott physics. *Rep. Prog. Phys.* **79**, 084502 (2016).
70. Scalapino, D. J. A common thread: the pairing interaction for unconventional superconductors. *Rev. Mod. Phys.* **84**, 1383–1417 (2012).
71. Pixley, J. H., Deng, L., Ingersent, K. & Si, Q. Pairing correlations near a Kondo-destruction quantum critical point. *Phys. Rev. B* **91**, 201109 (2015).
72. Cai, A., Pixley, J. H., Ingersent, K. & Si, Q. Critical local moment fluctuations and enhanced pairing correlations in a cluster Anderson model. *Phys. Rev. B* **101**, 014452 (2020).
73. Steglich, F. et al. Superconductivity in the presence of strong Pauli paramagnetism: $CeCu_2Si_2$. *Phys. Rev. Lett.* **43**, 1892–1896 (1979).
74. Stockert, O. et al. Magnetically driven superconductivity in $CeCu_2Si_2$. *Nat. Phys.* **7**, 119–124 (2011).
75. Stock, C., Broholm, C., Hudis, J., Kang, H. J. & Petrovic, C. Spin resonance in the *d*-wave superconductor $CeCoIn_5$. *Phys. Rev. Lett.* **100**, 087001 (2008).
76. Stockert, O., Kirchner, S., Steglich, F. & Si, Q. Superconductivity in Ce- and U-based '122' heavy-fermion compounds. *J. Phys. Soc. Jpn.* **81**, 011001 (2012).
77. Nica, E. M., Yu, R. & Si, Q. Orbital-selective pairing and superconductivity in iron selenides. *npj Quantum Mater.* **2**, 24 (2017).
78. Nica, E. M. & Si, Q. Multiorbital singlet pairing and $d+d$ superconductivity. *npj Quantum Mater*. (In the press).
79. Pang, G. et al. Fully gapped *d*-wave superconductivity in $CeCu_2Si_2$. *Proc. Natl Acad. Sci. USA* **115**, 5343–5347 (2018).
80. Yamashita, T. et al. Fully gapped superconductivity with no sign change in the prototypical heavy-fermion $CeCu_2Si_2$. *Sci. Adv.* **3**, e1601667 (2017).
81. Kittaka, S. et al. Multiband superconductivity with unexpected deficiency of nodal quasiparticles in $CeCu_2Si_2$. *Phys. Rev. Lett.* **112**, 067002 (2014).
82. Smidman, M. et al. Interplay between unconventional superconductivity and heavy-fermion quantum criticality: $CeCu_2Si_2$ versus $YbRh_2Si_2$. *Phil. Mag.* **98**, 2930–2963 (2018).
83. Ikeda, H., Suzuki, M.-T. & Arita, R. Emergent loop-nodal $s_{\pm}$-wave superconductivity in $CeCu_2Si_2$: similarities to the iron-based superconductors. *Phys. Rev. Lett.* **114**, 147003 (2015).
84. Li, Y. et al. Gap symmetry of the heavy fermion superconductor $CeCu_2Si_2$ at ambient pressure. *Phys. Rev. Lett.* **120**, 217001 (2018).
85. Schuberth, E. et al. Emergence of superconductivity in the canonical heavy-electron metal $YbRh_2Si_2$. *Science* **351**, 485–488 (2016).
86. Jiao, L. et al. Fermi surface reconstruction and multiple quantum phase transitions in the antiferromagnet $CeRhIn_5$. *Proc. Natl Acad. Sci. USA* **112**, 673–678 (2015).
87. Ronning, F. et al. Electronic in-plane symmetry breaking at field-tuned quantum criticality in $CeRhIn_5$. *Nature* **548**, 313–317 (2017).
88. Nisoli, C., Moessner, R. & Schiffer, P. Colloquium: Artificial spin ice: designing and imaging magnetic frustration. *Rev. Mod. Phys.* **85**, 1473–1490 (2013).
89. Si, Q. Global magnetic phase diagram and local quantum criticality in heavy fermion metals. *Physica B* **378-380**, 23–27 (2006).
90. Si, Q. Quantum criticality and global phase diagram of magnetic heavy fermions. *Phys. Status Solidi B* **247**, 476–484 (2010).
91. Coleman, P. & Nevidomskyy, A. Frustration and the Kondo effect in heavy fermion materials. *J. Low Temp. Phys.* **161**, 182–202 (2010).
92. Vojta, M. From itinerant to local-moment antiferromagnetism in Kondo lattices: adiabatic continuity versus quantum phase transitions. *Phys. Rev. B* **78**, 125109 (2008).
93. Pixley, J. H., Yu, R. & Si, Q. Quantum phases of the Shastry–Sutherland Kondo lattice: implications for the global phase diagram of heavy-fermion metals. *Phys. Rev. Lett.* **113**, 176402 (2014).
94. Sato, T., Assaad, F. F. & Grover, T. Quantum Monte Carlo simulation of frustrated Kondo lattice models. *Phys. Rev. Lett.* **120**, 107201 (2018).
95. Kurita, N. et al. Localized magnetic excitations in the fully frustrated dimerized magnet $Ba_2CoSi_2O_6Cl_2$. *Phys. Rev. Lett.* **123**, 027206 (2019).
96. Li, B. et al. Competing magnetic interactions in the antiferromagnetic topological insulator $MnBi_2Te_4$. *Phys. Rev. Lett.* **124**, 167204 (2020).
97. Nakatsuji, S. et al. Metallic spin-liquid behavior of the geometrically frustrated Kondo lattice $Pr_2Ir_2O_7$. *Phys. Rev. Lett.* **96**, 087204 (2006).
98. Kim, M. S. & Aronson, M. C. Heavy fermion compounds on the geometrically frustrated Shastry–Sutherland lattice. *J. Phys. Condens. Matter* **23**, 164204 (2011).
99. Fritsch, V. et al. Approaching quantum criticality in a partially geometrically frustrated heavy-fermion metal. *Phys. Rev. B* **89**, 054416 (2014).
100. Tokiwa, Y., Stingl, C., Kim, M.-S., Takabatake, T. & Gegenwart, P. Characteristic signatures of quantum criticality driven by geometrical frustration. *Sci. Adv.* **1**, e1500001 (2015).
101. Wu, L. S. et al. Orbital-exchange and fractional quantum number excitations in an *f*-electron metal, Yb_2Pt_2Pb. *Science* **352**, 1206–1210 (2016).
102. Zhao, H. et al. Quantum-critical phase from frustrated magnetism in a strongly correlated metal. *Nat. Phys.* **15**, 1261–1266 (2019).
103. Kavai, M. et al. Discovery of nanoscale phase coexistence of heavy Fermi-liquid and metallic spin-liquid in geometrically frustrated $Pr_2Ir_2O_7$. Preprint at https://arxiv.org/abs/2006.07424 (2020).
104. Stockert, O. et al. Magnetic frustration in a metallic fcc lattice. *Phys. Rev. Res.* **2**, 013183 (2020).
105. Tokiwa, Y., Ishikawa, J. J., Nakatsuji, S. & Gegenwart, P. Quantum criticality in a metallic spin liquid. *Nat. Mater.* **13**, 356–359 (2014).
106. Küchler, R. et al. Uniaxial stress tuning of geometrical frustration in a Kondo lattice. *Phys. Rev. B* **96**, 241110 (2017).
107. Friedemann, S. et al. Detaching the antiferromagnetic quantum critical point from the Fermi-surface reconstruction in $YbRh_2Si_2$. *Nat. Phys.* **5**, 465–469 (2009).
108. Custers, J. et al. Evidence for a non-Fermi-liquid phase in Ge-substituted $YbRh_2Si_2$. *Phys. Rev. Lett.* **104**, 186402 (2010).
109. Shishido, H. et al. Tuning the dimensionality of the heavy fermion compound $CeIn_3$. *Science* **327**, 980–983 (2010).
110. Ishii, T. et al. Tuning the magnetic quantum criticality of artificial Kondo superlattices $CeRhIn_5$/$YbRhIn_5$. *Phys. Rev. Lett.* **116**, 206401 (2016).
111. Takabayashi, Y. et al. The disorder-free non-BCS superconductor Cs_3C_{60} emerges from an antiferromagnetic insulator parent state. *Science* **323**, 1585 (2009).
112. Ramshaw, B. J. et al. Quasiparticle mass enhancement approaching optimal doping in a high-T_c superconductor. *Science* **348**, 317 (2015).
113. Hewson, A. C. & Meyer, D. Numerical renormalization group study of the Anderson–Holstein impurity model. *J. Phys.: Condens. Matter* **14**, 427–445 (2002).
114. Lüffe, M. C., Koch, J. & von Oppen, F. Theory of vibrational absorption sidebands in the coulomb-blockade regime of single-molecule transistors. *Phys. Rev. B* **77**, 125306 (2008).
115. Kalla, M., Chebrolu, N. R. & Chatterjee, A. Magneto-transport properties of a single molecular transistor in the presence of electron–electron and electron–phonon interactions and quantum dissipation. *Sci. Rep.* **9**, 16510 (2019).
116. Hotta, T. Enhanced Kondo effect in an electron system dynamically coupled with local optical phonons. *J. Phys. Soc. Jpn* **76**, 084702 (2007).
117. Prokofiev, A. et al. Thermopower enhancement by encapsulating cerium in clathrate cages. *Nat. Mater.* **12**, 1096–1101 (2013).
118. Haldane, F. Nobel Lecture: Topological quantum matter. *Rev. Mod. Phys.* **89**, 040502 (2017).
119. Hasan, M. Z. & Kane, C. L. Colloquium: Topological insulators. *Rev. Mod. Phys.* **82**, 3045–3067 (2010).
120. Qi, X.-L. & Zhang, S.-C. Topological insulators and superconductors. *Rev. Mod. Phys.* **83**, 1057–1110 (2011).
121. Focus Issue: Topological semimetals. *Nat. Mater.* **15** (11) (2016).
122. Bansil, A., Lin, H. & Das, T. Colloquium: Topological band theory. *Rev. Mod. Phys.* **88**, 021004 (2016).
123. Armitage, N. P., Mele, E. J. & Vishwanath, A. Weyl and Dirac semimetals in three-dimensional solids. *Rev. Mod. Phys.* **90**, 015001 (2018).

124. Chiu, C.-K., Teo, J. C. Y., Schnyder, A. P. & Ryu, S. Classification of topological quantum matter with symmetries. *Rev. Mod. Phys.* **88**, 035005 (2016).
125. Po, H. C., Vishwanath, A. & Watanabe, H. Symmetry-based indicators of band topology in the 230 space groups. *Nat. Commun.* **8**, 50 (2017).
126. Zhang, T. et al. Catalogue of topological electronic materials. *Nature* **566**, 475–479 (2019).
127. Vergniory, M. G. et al. A complete catalogue of high-quality topological materials. *Nature* **566**, 480–485 (2019).
128. Tang, F., Po, H. C., Vishwanath, A. & Wan, X. Comprehensive search for topological materials using symmetry indicators. *Nature* **566**, 486–489 (2019).
129. Frantzeskakis, E. et al. Trigger of the ubiquitous surface band bending in 3D topological insulators. *Phys. Rev. X* **7**, 041041 (2017).
130. Huang, X. et al. Observation of the chiral-anomaly-induced negative magnetoresistance in 3D Weyl semimetal TaAs. *Phys. Rev. X* **5**, 031023 (2015).
131. Moll, P. J. W. et al. Transport evidence for Fermi-arc-mediated chirality transfer in the Dirac semimetal Cd_3As_2. *Nature* **535**, 266–270 (2016).
132. Zhang, C.-L. et al. Signatures of the Adler–Bell–Jackiw chiral anomaly in a Weyl fermion semimetal. *Nat. Commun.* **7**, 10735 (2016).
133. Zhang, C. et al. Quantum Hall effect based on Weyl orbits in Cd_3As_2. *Nature* **565**, 331–336 (2019).
134. Shao, Y. et al. Electronic correlations in nodal-line semimetals. *Nat. Phys.* **16**, 636–641 (2020).
135. Tang, H.-K. et al. The role of electron–electron interactions in two-dimensional Dirac fermions. *Science* **361**, 570–574 (2018).
136. Grefe, S. E., Lai, H.-H., Paschen, S. & Si, Q. Weyl–Kondo semimetals in nonsymmorphic systems. *Phys. Rev. B* **101**, 075138 (2020).
137. Dzsaber, S. et al. Giant spontaneous Hall effect in a nonmagnetic Weyl–Kondo semimetal. Preprint at https://arxiv.org/abs/1811.02819 (2018).
138. Dzsaber, S. et al. Quenching a Weyl–Kondo semimetal by magnetic field. Preprint at https://arxiv.org/abs/1906.01182 (2019).
139. Guo, C. et al. Possible Weyl fermions in the magnetic Kondo system CeSb. *npj Quantum Mater.* **2**, 39 (2017).
140. Guo, C. Y. et al. Evidence for Weyl fermions in a canonical heavy-fermion semimetal YbPtBi. *Nat. Commun.* **9**, 4622 (2018).
141. Schoop, L. M. et al. Tunable Weyl and Dirac states in the nonsymmorphic compound CeSbTe. *Sci. Adv.* **4**, eaar2317 (2018).
142. Zhai, L.-J., Chou, P.-H. & Mou, C.-Y. Magnetic phases and unusual topological electronic structures of Weyl semimetals in strong interaction limit. *Phys. Rev. B* **94**, 125135 (2016).
143. Xu, Y., Yue, C., Weng, H. & Dai, X. Heavy Weyl fermion state in $CeRu_4Sn_6$. *Phys. Rev. X* **7**, 011027 (2017).
144. Roy, B., Goswami, P. & Juričić, V. Interacting Weyl fermions: phases, phase transitions, and global phase diagram. *Phys. Rev. B* **95**, 201102 (2017).
145. Chang, P.-Y. & Coleman, P. Parity-violating hybridization in heavy Weyl semimetals. *Phys. Rev. B* **97**, 155134 (2018).
146. Ivanov, V., Wan, X. & Savrasov, S. Y. Topological insulator-to-Weyl semimetal transition in strongly correlated actinide system UNiSn. *Phys. Rev. X* **9**, 041055 (2019).
147. Lu, Y.-W., Chou, P.-H., Chung, C.-H. & Mou, C.-Y. Tunable topological semimetallic phases in Kondo lattice systems. *Phys. Rev. B* **99**, 035141 (2019).
148. Wang, L.-J. Spatial anisotropy of the Kondo screening cloud in a type-II Weyl semimetal. *Phys. Rev. B* **99**, 235108 (2019).
149. Yang, Y.-Y., Deng, M.-X., Duan, H.-J., Luo, W. & Wang, R.-Q. Electrically tunable Kondo effect as a direct measurement of the chiral anomaly in disordered Weyl semimetals. *Phys. Rev. B* **101**, 205137 (2020).
150. Grefe, S. E., Lai, H.-H., Paschen, S. & Si, Q. Weyl–Kondo semimetal: towards control of Weyl nodes. *JPS Conf. Proc.* **30**, 011013 (2020).
151. Joshi, D., Li, C., Tarnopolsky, G., Georges, A. & Sachdev, S. Deconfined critical point in a doped random quantum Heisenberg magnet. *Phys. Rev. X* **10**, 021033 (2020).
152. Cha, P., Wentzell, N., Parcollet, O., Georges, A. & Kim, E. Linear resistivity and Sachdev–Ye–Kitaev (SYK) spin liquid behavior in a quantum critical metal with spin-1/2 fermions. *Proc. Natl Acad. Sci. USA* **117**, 18341–18346 (2020)
153. Senthil, T. Critical Fermi surfaces and non-Fermi liquid metals. *Phys. Rev. B* **78**, 035103 (2008).
154. Terletska, H., Vučičević, J., Tanasković, D. & Dobrosavljević, V. Quantum critical transport near the Mott transition. *Phys. Rev. Lett.* **107**, 026401 (2011).
155. Jia, Y. et al. Mott transition and superconductivity in quantum spin liquid candidate $NaYbSe_2$. *Chin. Phys. Lett.* **37**, 097404 (2020).
156. Pépin, C. Selective Mott transition and heavy fermions. *Phys. Rev. B* **77**, 245129 (2008).
157. Anisimov, V., Nekrasov, I., Kondakov, D., Rice, T. & Sigrist, M. Orbital-selective Mott-insulator transition in $Ca_{2-x}Sr_xRuO_4$. *Eur. Phys. J. B* **25**, 191–201 (2002).
158. Yu, R. & Si, Q. Orbital-selective Mott phase in multiorbital models for iron pnictides and chalcogenides. *Phys. Rev. B* **96**, 125110 (2017).
159. Kang, M. et al. Dirac fermions and flat bands in the ideal kagome metal FeSn. *Nat. Mater.* **19**, 163–169 (2020).
160. Yao, M. et al. Switchable Weyl nodes in topological Kagome ferromagnet Fe_3Sn_2. Preprint at https://arxiv.org/abs/1810.01514 (2018).
161. Bistritzer, R. & MacDonald, A. H. Moiré bands in twisted double-layer graphene. *Proc. Natl. Acad. Sci. USA* **108**, 12233–12237 (2011).
162. Yankowitz, M. et al. Tuning superconductivity in twisted bilayer graphene. *Science* **363**, 1059 (2019).
163. Lu, X. et al. Superconductors, orbital magnets and correlated states in magic-angle bilayer graphene. *Nature* **574**, 653–657 (2019).
164. Kerelsky, A. et al. Maximized electron interactions at the magic angle in twisted bilayer graphene. *Nature* **572**, 95–100 (2019).
165. Choi, Y. et al. Electronic correlations in twisted bilayer graphene near the magic angle. *Nat. Phys.* **15**, 1174–1180 (2019).
166. Chen, L., Hu, H. & Si, Q. Fragile insulator and electronic nematicity in a graphene moiré system. Preprint at https://arxiv.org/abs/2007.06086 (2020).
167. Wang, Q.-Y. et al. Interface-induced high-temperature superconductivity in single unit-cell FeSe films on $SrTiO_3$. *Chin. Phys. Lett.* **29**, 037402 (2012).
168. Lee, J. J. et al. Interfacial mode coupling as the origin of the enhancement of T_c in FeSe films on $SrTiO_3$. *Nature* **515**, 245–248 (2014).
169. Li, Z.-X., Devereaux, T. P. & Lee, D.-H. Electronic and phononic properties of a two-dimensional electron gas coupled to dipolar phonons via small-momentum-transfer scattering. *Phys. Rev. B* **100**, 241101 (2019).
170. Polshyn, H. et al. Large linear-in-temperature resistivity in twisted bilayer graphene. *Nat. Phys.* **15**, 1011–1016 (2019).
171. Giannetti, C. et al. Ultrafast optical spectroscopy of strongly correlated materials and high-temperature superconductors: a non-equilibrium approach. *Adv. Phys.* **65**, 58–238 (2016).
172. Fausti, D. et al. Light-induced superconductivity in a stripe-ordered cuprate. *Science* **331**, 189–191 (2011).
173. Cremin, K. A. et al. Photoenhanced metastable *c*-axis electrodynamics in stripe-ordered cuprate $La_{1.885}Ba_{0.115}CuO_4$. *Proc. Natl Acad. Sci. USA* **116**, 19875–19879 (2019).
174. Budden, M. et al. Evidence for metastable photo-induced superconductivity in K_3C_{60}. Preprint at https://arxiv.org/abs/2002.12835 (2020).
175. Brown, P. T. et al. Bad metallic transport in a cold atom Fermi–Hubbard system. *Science* **363**, 379–382 (2019).
176. Ozawa, T. et al. Topological photonics. *Rev. Mod. Phys.* **91**, 015006 (2019).
177. Islam, R. et al. Measuring entanglement entropy in a quantum many-body system. *Nature* **528**, 77–83 (2015).
178. Gegenwart, P. et al. Magnetic-field induced quantum critical point in $YbRh_2Si_2$. *Phys. Rev. Lett.* **89**, 056402 (2002).

Acknowledgements
The authors thank the late Elihu Abrahams, and P. Aynajian, P. Blaha, A. Cai, P. Coleman, J. Dai, W. Ding, S. Dzsaber, G. Eguchi, S. Friedemann, P. Goswami, S. Grefe, K. Grube, K. Held, H. Hu, K. Ingersent, S. Kirchner, J. Kono, H.-H. Lai, C.-C. Liu, Y. Luo, V. Martelli, E. Morosan, A. Nevidomskyy, D. H. Nguyen, E. Nica, J. Pixley, L. Prochaska, A. Prokofiev, E. Schuberth, A. Severing, T. Shiroka, F. Steglich, O. Stockert, L. Sun, P. Sun, M. Taupin, J. D. Thompson, J. Tomczak, H. von Löhneysen, S. Wirth, J. Wu, Z. Xu, X. Yan, R. Yu, H. Yuan, J.-X. Zhu and D. Zocco for collaborations and/or discussions. The work has been supported in part by the Austrian Science Fund grants no. P29279-N27, P29296-N27 and DK W1243, the European Union's Horizon 2020 Research and Innovation Programme grant EMP-824109 (S.P.), the US National Science Foundation (NSF) grant no. DMR-1920740 and the Robert A. Welch Foundation grant no. C-1411 (Q.S.). We acknowledge the hospitality of the Aspen Center for Physics, which is supported by NSF grant no. PHY-1607611.

Author contributions
The authors contributed equally to all aspects of the article.

Competing interests
The authors declare no competing interests.

Peer review information
Nature Reviews Physics thanks Yuji Matsuda and the other, anonymous, reviewers for their contribution to the peer review of this work.

Publisher's note
Springer Nature remains neutral with regard to jurisdictional claims in published maps and institutional affiliations.

Supplementary information
Supplementary information is available for this paper at https://doi.org/10.1038/s42254-020-00262-6.

nature research

https://doi.org/10.1038/s42254-020-00262-6

Supplementary information

Quantum phases driven by strong correlations

In the format provided by the authors and unedited

Supplementary Figure

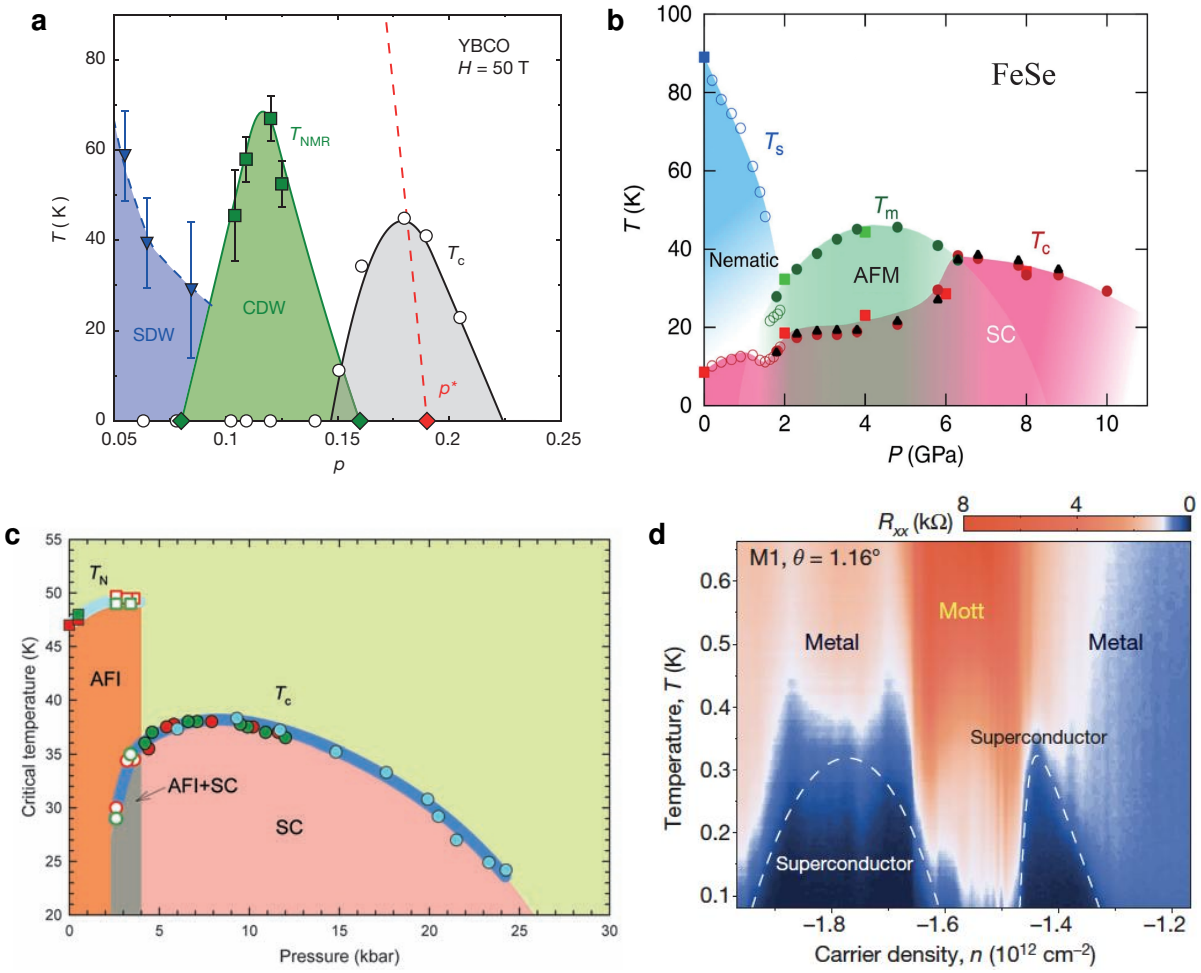

Figure S1. Landscape of quantum phases in strongly correlated materials. a-d| Temperature-tuning parameter phase diagrams of the cuprate superconductor $YBaCuO_{6-\delta}$ (reproduced with permission from ref. 1), the iron pnictide FeSe (adapted with permission from ref. 179), the fulledide compound C_{60} (reproduced with permission from ref. 111), and magic angle twisted bilayer graphene (reproduced with permission from ref. 10), respectively. The different phases and functionalities result from the interplay of various low-energy degrees of freedom as illustrated in Fig. 1 of the main part.

Supplementary Boxes

InfoBox 1: **Heavy fermion state out of Kondo lattice**

Heavy fermion materials contain elements with partially-filled f electrons, which are coupled to *spd* electrons through a hybridization matrix[27]. In many cases, the count of the f electrons is fixed at an odd-integer value, because a change of their valence occupation costs too much Coulomb repulsion. For example, there would be one $4f$ electron per Ce ion or thirteen $4f$ electrons (which is equivalent to one $4f$ hole) per Yb ion. In such cases, an f electron acts as a localized magnetic moment in the low-energy description. We illustrate the physics in the simplest situation, with one spin-1/2 local moment occupying each site, each unit containing only one site, and only one *spd* based conduction electron band. This is the Kondo lattice Hamiltonian, which reads

$$\begin{aligned} \mathcal{H}_{\rm KL} &= \mathcal{H}_f + \mathcal{H}_K + \mathcal{H}_c, \\ \mathcal{H}_f &= (1/2)\sum_{ij} I_{ij}\ \mathbf{S}_i\ \mathbf{S}_j\,; \qquad \mathcal{H}_K = \sum_i J_{\rm K}\ \mathbf{S}_i \cdot \mathbf{s}_{c,i}\,; \qquad \mathcal{H}_c = \sum_{\mathbf{k}\sigma} \epsilon_{\mathbf{k}} c^\dagger_{\mathbf{k}\sigma} c_{\mathbf{k}\sigma} \end{aligned} \tag{1}$$

At a site i, the local moment, $\mathbf{S}_i$ interacts with the spin of the conduction electron, $\mathbf{s}_{c,i} = (1/2) c_i^\dagger \vec{\sigma} c_i$, through an antiferromagnetic Kondo exchange coupling $J_{\rm K}$. It is convenient to introduce an explicit term, I_{ij}, to describe the RKKY interaction between the local moments located at different sites. Finally, $\epsilon_{\mathbf{k}}$ describes the band dispersion of the conduction c electrons. The model can be generalized to incorporate additional complexity.

For the Hamiltonian 1, the Kondo coupling can be parameterized by a bare Kondo energy scale, $T_0 = N_{\rm F}^{-1} \exp\left(-1/J_{\rm K} N_{\rm F}\right)$ (with $k_{\rm B}$ being set to unity), where $N_{\rm F}$ is the density of states of the noninteracting conduction electron band at the Fermi energy [the corresponding Fermi wavevector being marked $k_{\rm F}$ in (Fig. 4a)]. The RKKY interaction I_{ij} is taken to have a characteristic value I. The Doniach competition[28] is characterized by tuning the parameter $\delta = T_0/I$. Where T_0 dominates over I is the regime for the traditional description of a paramagnetic heavy Fermi liquid. In the ground state, the local moments and the spins of conduction electrons form a Kondo singlet. To describe the excitation spectrum associated with this ground state, it is convenient to rewrite the Kondo interaction at any given site to be $(1/2)\sum_\sigma [\sigma S^z c^\dagger_\sigma + X^{\sigma\bar{\sigma}} c^\dagger_{\bar{\sigma}}] c_\sigma$, where $\bar{\sigma} \equiv -\sigma$, and $X^{\sigma\bar{\sigma}}$ is the spin raising (lowering) operator for

$\sigma =\uparrow (\downarrow)$. With a nonzero static amplitude for such a Kondo singlet, the local moment binds with the conduction electron, and $F_\sigma^\dagger = \sigma S^z c_\sigma^\dagger + X^{\sigma\bar{\sigma}} c_{\bar{\sigma}}^\dagger$ acts as a composite fermion. The Kondo interaction becomes a hybridization $\sum_\sigma F_\sigma^\dagger c_\sigma$. From the perspective of the conduction electrons, $F_\sigma^\dagger$ introduces a resonance near the Fermi energy. Thus, $F_\sigma^\dagger$ is referred to as creating a Kondo resonance. In the overall electronic excitations, the composite fermion hybridizes with the conduction electron band to form the hybridized bands sketched in Fig. 4a[27]. The Fermi surface is formed by both the composite fermions and the conduction electrons, and the Fermi surface (corresponding to the Fermi wavevector $k_{\rm F}^*$) becomes large. The composite fermions lead to a density of states with a sharp peak near the Fermi energy (see Fig. 4b), which spreads over a narrow energy range determined by the Kondo scale.

The scale T_0 is also reflected in the evolution of the excitation spectrum as a function of temperature. At temperatures much larger than T_0, the local moments and conduction electrons are essentially decoupled. As temperature is lowered through T_0, the Kondo correlation between the two species of spins start to set in. This leads to the initial onset of a "hybridization gap", as would be seen in the optical conductivity $\sigma(\omega)$ (see Fig. 4c). The corresponding frequency scale is $\sqrt{T_0 D}$ (where D is the conduction electron bandwidth) is determined by the zero-wavevector (direct) transfer transition between the occupied and empty states in the hybridized bands.

InfoBox 2: **Noninteracting electronic topology.**

Weyl semimetals are materials in which bulk energy bands touch only at discrete points in momentum space (the Weyl nodes) and where, in the vicinity of the nodes, the electron wave functions of these two bands can be approximated by the Weyl equation, which has far-reaching consequences. In the pertinent lattice theory of chirally invariant fermions with locality, there is an equal number of production and annihilation of Weyl fermions[180]. Thus, Weyl nodes with Weyl fermions of opposite chirality occur in pairs such that the axial charge is conserved. The nontrivial topological nature of a Weyl semimetal guarantees that the two nodes of such a pair are separated in momentum space. Experimental observables include the linear bulk dispersion near the Weyl nodes, surface Fermi arcs that connect the projection of two bulk Weyl nodes of different chirality in the surface Brillouin zone, the chiral anomaly manifesting in an extremely large negative longitudinal magnetoresistance, or the monopoles and antimonopoles of Berry flux in momentum space leading to spontaneous or anomalous Hall responses. Space group symmetry plays an important role in the emergence of Weyl nodes in a robust way[125,181,182]. ARPES is playing a key role in the identification of weakly-interacting topological electronic materials. As a highly surface sensitive technique it is particularly well suited to probe topological surface states. Indeed, an APRES investigation of the (111) surface of the topological insulator Bi_2Se_3 revealed, with amazing clarity, a single Dirac cone in the surface electronic band dispersion (**a**, adapted with permission from ref. 183). If higher energy photons are used, ARPES acquires some bulk sensitivity. It has thus also been used to probe topological bulk bands. Examples are the identification of a bulk Dirac cone in Na_3Bi (**b**, adapted with permission from ref. 184) and of two closely spaced Weyl cones in TaAs (**c**, adapted with permission from ref. 185). In the latter, crescent-shaped surface states (**d**, adapted with permission from ref. 185) were assigned as being the topological Fermi arcs that connect the surfaces projections of the bulk Weyl nodes (+ and − in panel **c**). That there are two arcs is attributed to two pairs of bulk nodes collapsing in the surface projection.

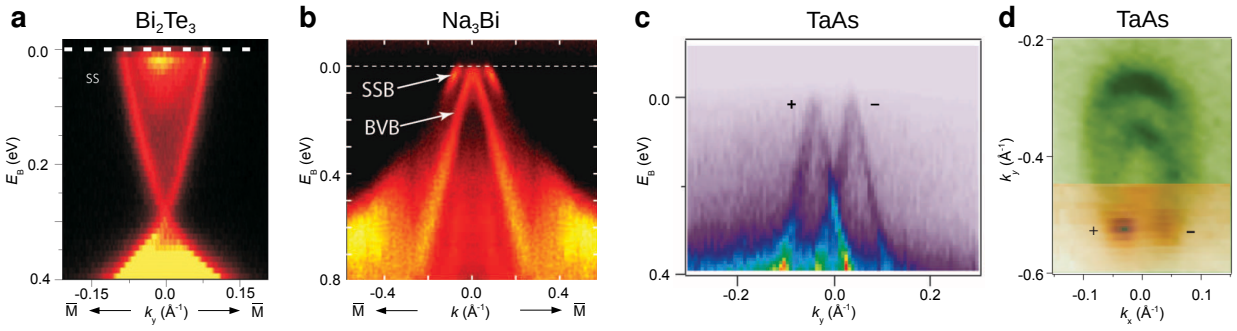

1. Badoux, S., Tabis, W., Laliberté, F., Grissonnanche, G., Vignolle, B., Vignolles, D., Béard, J., Bonn, D. A., Hardy, W. N., Liang, R., Doiron-Leyraud, N., Taillefer, L. & Proust, C. Change of carrier density at the pseudogap critical point of a cuprate superconductor. *Nature* **531**, 210 (2016).

10. Cao, Y., Fatemi, V., Fang, S., Watanabe, K., Taniguchi, T., Kaxiras, E. & Jarillo-Herrero, P. Unconventional superconductivity in magic-angle graphene superlattices. *Nature* **556**, 43 (2018).

27. Hewson, A. C. *The Kondo Problem to Heavy Fermions* (Cambridge University Press, Cambridge, 1997).

28. Doniach, S. The Kondo lattice and weak antiferromagnetism. *Physica B+C* **91**, 231 (1977).

111. Takabayashi, Y., Ganin, A. Y., Jeglič, P., Arčon, D., Takano, T., Iwasa, Y., Ohishi, Y., Takata, M., Takeshita, N., Prassides, K. & Rosseinsky, M. J. The disorder-free non-BCS superconductor Cs_3C_{60} emerges from an antiferromagnetic insulator parent state. *Science* **323**, 1585 (2009).

125. Po, H. C., Vishwanath, A. & Watanabe, H. Symmetry-based indicators of band topology in the 230 space groups. *Nat. Commun.* **8**, 50 (2017).

179. Sun, J. P., Matsuura, G. Z., K. Ye, Mizukami, Y., Shimozawa, M., Matsubayashi, K., Yamashita, M., Watashige, T., Kasahara, S., Matsuda, Y., Yan, J. Q., Sales, B. C., Uwatoko, Y., Cheng, J. G. & Shibauchi, T. Dome-shaped magnetic order competing with high-temperature superconductivity at high pressures in FeSe. *Nat. Commun.* **7**, 12146 (2016).

180. Nielsen, H. B. & Ninomiya, M. The Adler-Bell-Jackiw anomaly and Weyl fermions in a crystal. *Phys. Lett. B* **130**, 389 (1983).

181. Young, S. M., Zaheer, S., Teo, J. C. Y., Kane, C. L., Mele, E. J. & Rappe, A. M. Dirac semimetal in three dimensions. *Phys. Rev. Lett.* **108**, 140405 (2012).

182. Cano, J., Bradlyn, B., Wang, Z., Elcoro, L., Vergniory, M. G., Felser, C., Aroyo, M. I. & Bernevig, B. A. Building blocks of topological quantum chemistry: Elementary band representations. *Phys. Rev. B* **97**, 035139 (2018).

183. Xia, Y., Qian, D., Hsieh, D., Wray, L., Pal, A., Lin, H., Bansil, A., Grauer, D., Hor, Y. S., Cava, R. J. & Hasan, M. Z. Observation of a large-gap topological-insulator class with a single

Dirac cone on the surface. *Nature Phys.* **5**, 398 (2009).

184. Liu, Z. K., Zhou, B., Zhang, Y., Wang, Z. J., Weng, H. M., Prabhakaran, D., Mo, S.-K., Shen, Z. X., Fang, Z., Dai, X., Hussain, Z. & Chen, Y. L. Discovery of a three-dimensional topological Dirac semimetal, Na_3Bi. *Science* **343**, 864 (2014).

185. Xu, S.-Y., Belopolski, I., Alidoust, N., Neupane, M., Bian, G., Zhang, C., Sankar, R., Chang, G., Yuan, Z., Lee, C.-C., Huang, S.-M., Zheng, H., Ma, J., Sanchez, D. S., Wang, B., Bansil, A., Chou, F., Shibayev, P. P., Lin, H., Jia, S. & Hasan, M. Z. Discovery of a Weyl fermion semimetal and topological Fermi arcs. *Science* **349**, 613 (2015).